INL/EXT-21-64809

Advanced Reactor Technologies: Gas-Cooled Reactor Third Quarter 2021 Report

April, May, June 2021

Please note this report contains preliminary data, interim conclusions, and observations from work-in-progress.

Idaho National Laboratory

INL is a U.S. Department of Energy National Laboratory operated by Battelle Energy Alliance, LLC

INL/EXT-21-64809

Advanced Reactor Technologies: Gas-Cooled Reactor Third Quarter 2021 Report

April, May, June 2021

Idaho National Laboratory
INL ART Program
Idaho Falls, Idaho 83415

http://www.art.inl.gov

Prepared for the
U.S. Department of Energy
Office of Nuclear Energy
Under DOE Idaho Operations Office
Contract DE-AC07-05ID14517

Page intentionally left blank

INL ART Program

Advanced Reactor Technologies: Gas-Cooled Reactor Third Quarter 2021 Report

INL/EXT-21-64809

April, May, June 2021

Approved by:

Travis Mitchell

Travis R. Mitchell
INL ART Program Manager

10/25/2021

Date

Page intentionally left blank

CONTENTS

FIGURES

TABLES

Page intentionally left blank

ACRONYMS

AGC	Advanced Graphite Creep
AGR	Advanced Gas Reactor
ANL	Argonne National Laboratory
ANS	American Nuclear Society
ART	Advanced Reactor Technologies
ASME	American Society of Mechanical Engineers
ASTM	American Society for Testing and Materials
ATR	Advanced Test Reactor
BPVC	Boiler and Pressure Vessel Code
DOE	Department of Energy
FITT	Furnace for Irradiated TRISO Testing
FY	Fiscal Year
GIF	Generation IV International Forum
HDG	High dose Graphite
HFEF	Hot Fuel Examination Facility
HTTF	High Temperature Test Facility
HTGR	High Temperature Gas Cooled reactor
HTR	high temperature reactor
HRTEM	high-resolution transmission electron microscopy
IFEL	Irradiated Fuels Examination Laboratory
IMGA	Irradiated Microsphere Gamma Analyzer
INGSM	International Nuclear Graphite Specialist Meeting
INL	Idaho National Laboratory
IR	inner ring
LFA	Laser Flash
MSR	Molten Salt Reactor
NDM	Nonmetallic Design and Materials
NSTF	Natural Convection Shutdown Heat-Removal Test Facility
OPyC	outer pyrolytic
OR	outer ring
ORNL	Oak Ridge National Laboratory
OSU	Oregon State University
PCC	Pressurized Conduction Cooldown

PIE	post-irradiation examination
PGS	Precision Gamma Scanner
PM	parabolic mirrors
PMB	Project Management Board
PTR	photothermal radiometry
R&D	Research and Development
SiC	silicon carbide
SRF	stress rupture factor
SRNL	Savannah River National Laboratory
TEM	Transmission electron microscopy
TRISO	tristructural isotropic
UCO	Uranium carbide/oxide
WG	Working group
XCT	X-ray computed tomography

Advanced Reactor Technologies: Gas-Cooled Reactor Third Quarter 2021 Report

1. MAJOR ACCOMPLISHMENTS

1.1 Fuels Development

Highlights of Advanced Gas Reactor (AGR) fuels-development activities during April, May and June 2021 are as follows:

April

- Completed a second 50 h, 1400°C oxidation test in the Oak Ridge National Laboratory (ORNL) Furnace for Irradiated tristructural isotropic (TRISO) Testing (FITT) of 10 unirradiated and 10 irradiated AGR-2 Uranium carbide/oxide (UCO) TRISO particles with the outer pyrolytic (OPyC) layer previously removed to expose the silicon carbide (SiC) surface to the oxidizing environment in the FITT.
- Completed gamma counting with the ORNL Irradiated Microsphere Gamma Analyzer (IMGA) of the 10 irradiated particles from the second 50 h oxidation test in the FITT, no particles indicated through-layer SiC failure.
- Completed 100 h, 1400°C FITT oxidation test of unirradiated and irradiated AGR-2 UCO TRISO particles with OPyC removed, and specimen unloading is in progress.
- Completed crush-burn-leach of a random sample of 200 AGR-3/4 Compact 1-4 driver fuel particles to dissolve kernels in nitric acid and acquire aliquots of the leachate for average burnup analysis and transferred aliquots from the ORNL Irradiated Fuels Examination Laboratory (IFEL) hot cells to the ORNL Nuclear Analytical Chemistry & Isotopics Laboratory (NACIL).
- Completed bench testing of new rotisserie platform for AGR-3/4 radial deconsolidation, loaded platform into the IFEL hot cells, and assembled the radial deconsolidation rig.
- Completed radial deconsolidation of AGR-3/4 Compact 7-4 in the IFEL hot cell and completed the preburn leaching of the first segment.
- Completed elemental analyses of fission product distributions in randomly selected AGR-3/4 Compact 1-4 and Compact 10-4 driver fuel particles using energy dispersive x-ray spectroscopy (EDS) in the ORNL TRISO particle scanning electron microscope.
- Received shipment of the second half of the irradiated AGR-5/6/7 test train, containing Capsule 3, 4, and 5, at the Hot Fuels Examination Facility (HFEF).
- Performed visual examination of the first half of the irradiated AGR-5/6/7 test train, containing Capsule 1 and 2.
- Received notification from Savanah River National Laboratory (SRNL) that irradiated AGR-5/6/7 compacts has been approved for shipment in the 9977 shipping containers.
- Shipped four (4) 9977 shipping containers to SRNL for re-certification in preparation for shipping AGR-5/6/7 compacts to ORNL.
- Completed radial deconsolidation of AGR-3/4 compact 10-3 in the Analytical Laboratory at Idaho National Laboratory (INL).
- Completed disposal of residual materials from TRISO fuels development at BWX Technologies Nuclear Operations Group containing natural uranium.

May

- Completed 200 h, 1400°C oxidation test in the ORNL FITT of 10 unirradiated and 10 irradiated AGR-2 UCO TRISO particles with the OPyC layer previously removed to expose the SiC surface to the oxidizing environment in the FITT.
- Completed gamma counting with the ORNL IMGA of the irradiated particles from a 100 h oxidation test in the FITT.
- Completed burn-leach of the middle segment and the outermost segment from radially deconsolidated AGR-3/4 Compact 7-4 in the ORNL IFEL hot cell, and survey of driver fuel particles from this segment is in progress with the IMGA to measure individual cesium, cerium, and ruthenium inventories to determine if the SiC in any particle failed to retain fission products as expected.
- Completed gamma scanning of the first segment of the AGR-5/6/7 test train (containing Capsules 1 and 2) using the Precision Gamma Scanner (PGS) at INL.
- Received corrected Sr-90 values from Pacific Northwest National Laboratory for the samples from AGR-3/4 rings physical sampling and incorporated them into a new report that will be released in early June.

June

- Completed 400 h, 1400°C oxidation test in the ORNL FITT of 10 unirradiated and 10 irradiated AGR-2 UCO Compact 5-4-2 particles with the OPyC layer previously removed to expose the SiC surface to the oxidizing environment.
- Completed analysis of oxide layer on selected AGR-2 UCO Compact 5-4-2 particles from the 50 h and 100 h oxidation tests at 1400°C in the FITT using a scanning electron microscope to determine oxide thickness after milling radial profiles with a focused ion beam (FIB). Lamella from selected particles were also prepared with the FIB for scanning transmission electron microscopy to allow for high resolution analysis of the oxide layer.
- Completed and issued a report on destructive sampling, radiochemical analyses, and construction of fission product radial concentration profiles in the AGR-3/4 rings. These results are currently being compared to the non-destructive gamma tomography results. This work will be the basis for back-calculating fission product transport parameters and performing model refinements and comparisons.
  John D. Stempien. 2021. "Measurement of Fission Product Concentration Profiles in AGR-3/4 TRISO Fuel Graphitic Matrix and Nuclear Graphites." INL/EXT-21-628632, Idaho National Laboratory.
- Completed all the radiochemical analyses from radial deconsolidation of AGR-3/4 Compact 8-2 at INL.
- Completed radial deconsolidation of AGR-3/4 Compact 7-4 in the ORNL IFEL hot cell.
- Completed high-accuracy quantitative analyses at the ORNL NACIL for stable uranium, plutonium, and neodymium isotopes in aliquots acquired from dissolved kernels taken from AGR-3/4 Compact 1-4; these data will be processed to determine the average burnup in the driver fuel particles.
- Completed preparation of cracked particles from AGR-2 Compact 2-2-1 at ORNL and confirmed via x-ray computed tomography (XCT) that the desired crack morphologies had been produced. All 10 particles will be shipped from ORNL to INL for the reirradiation-heating tests.
- Completed exterior visual examinations, PGS, and neutron radiography of Capsules 1 and 2 of the AGR-5/6/7 irradiation experiment at INL. Nothing unusual was observed. Gamma scanning and neutron radiography indicate no gross fuel relocation occurred.

- Completed neutron radiography of AGR-5/6/7 Capsules 3, 4, and 5 at INL.
- Completed Phase II remote qualifications of AGR-5/6/7 component leaching and disassembly equipment at INL.
- Completed recertification of the 9977 containers at SRNL and SRNL sent the containers back to INL. These containers will be used to ship AGR-5/6/7 compacts from INL to ORNL.
- Initiated disposal of residual low-enriched uranium materials stored at BWXT- Nuclear Operations Group that are not of interest to other programs or the Central Scrap Management Office.

1.2 High-Temperature Materials Development

Highlights of high-temperature materials activities during April, May and June 2021 are as follows:

April

- Sustained and interrupted long-term creep-rupture testing (800°C, 35 MPa) of a base-metal V-notch specimen. The expected life is 100,000 hours. The test was interrupted at 28,812 hours for XCT characterization.
- Sustained and interrupted long-term creep-rupture testing (800°C, 35 MPa) of a weld-metal V-notch specimen. The expected life is 100,000 hours. The test was interrupted at 21,739 hours for XCT characterization.
- Corrected feedback issues in the compact tension testing system and identified a dummy specimen to be used for quantitative verification of the system.
- Submitted a machining request to Fabrication Services to get Alloy 617 compact tension specimens machined.
- Performed metallography and characterization on seven of the cyclic cross-weld specimens with Alloy 617 base and filler metal. For all seven specimens the weld was centered with respect to the extensometer and reduced section. At least one of each condition tested was characterized. The primary crack for all seven specimens was in the weld metal.
- Submitted an iBuy request to procure UTP A 2133 Mn weld wire.

May

- Provided an update of the plans on the tertiary creep-based criterion during the May Allowable Stress Criteria meeting in preparation for voting on the proposal.
- Participated in the May American Society of Mechanical Engineers (ASME) Boiler and Pressure Vessel Code (BPVC) Week which was held virtually and provided updates on ongoing work.
- Collected and analyzed XCT data from the notch and straight gauge of a base-metal V-notch specimen which was interrupted approximately 28,812 hours into an 800°C, 35 MPa creep-rupture test. This test has a 100,000-hour estimated rupture life.
- Collected and analyzed XCT data collected from the notch and straight gauge of a weld-metal V-notch specimen which was interrupted approximately 21,739 hours into an 800°C, 35 MPa creep-rupture test. This test has a 100,000-hour estimated rupture life.
- Analyzed XCT data from the straight gauge of a ruptured baseline base-metal Alloy 617 V-notch creep-rupture (800°C, 65.3 MPa) specimen.
- Analyzed the XCT data from the straight gauge and notch of an interrupted base-metal baseline creep-rupture specimen. The test conditions for this creep-rupture test are 800°C and 60 MPa. This

data was collected after 2,000 hours of testing. The data collected after 1,000 hours of testing was reanalyzed to detect creep damage at the surface of the specimen.

- Performed a verification test of the crack growth experimental setup by running a dummy specimen in air. No major issues were observed during this system verification test.
- Worked with Fabrication Services to get Alloy 617 compact-tension specimens machined.
- Interrupted creep-rupture testing (850°C, 54 MPa) of diffusion-welded Alloy 617. The test was interrupted at 1,030 hours.
- Started and sustained creep-rupture testing (850°C, 54 MPa) of diffusion-welded Alloy 617. The test is currently at 309 hours. The test will be interrupted at approximately 750 hours.

June

- Interviewed and hired two postdoctoral researchers.
- Attended the June powder metallurgy hot isostatic pressing process group meeting. This group is a subset of the Task Group Advanced Manufacturing committee.
- Reloaded and restarted the interrupted long-term creep-rupture test (800°C, 35 MPa) of a base-metal V-notch specimen. The expected life is 100,000 hours. The test is currently at 29,056 hours.
- Collected XCT data from the notch and straight gauge of a weld-metal V-notch specimen prior to creep-rupture testing. The specimen will be tested at 800°C with an initial applied stress of 35 MPa.
- Started an interrupted long-term creep-rupture test (800°C, 35 MPa) of a weld-metal V-notch specimen. The expected life is 100,000 hours. The test is currently at 41 hours.
- Attended the Office of Nuclear Reactor Deployment Advanced Materials Research and Development (R&D) Program Review.
- Presented on “Notch Effect Testing and A800H Weldment” at the Nuclear Reactor Deployment Advanced Materials R&D Program Review.
- Transferred Alloy 617 plate to an North Holmes Laboratory facility for machining and completed a consultation with a fabrication technician to confirm machining requirements.
- Interrupted creep-rupture testing (850°C, 54 MPa) of diffusion-welded Alloy 617. The test was interrupted after 750 hours of testing.
- Received the UTP A 2133 Mn weld wire at INL. The weld wire was inspected and green tagged.
- Drafted a report titled “Assessment of Overmatched Filler (Alloy 617) to Improve Alloy 800H Stress Rupture Factors.” This report is the deliverable for milestone M3AT-21IN060405.

1.3 Graphite

Highlights of graphite activities during April, May and June 2021 are as follows:

April

- Completed primary removal of creep and un-stressed Advanced Graphite Creep (AGC)-4 graphite samples from the graphite body and packaged them for survey and transport.
- Performed milling to remove recalcitrant center stack piggyback samples from AGC-4.
- Set up equipment for measurement of segments of graphite body for overall length determination, surveyed creep sample transfer tubes, and set up equipment for recovery of fluence monitor capsules.

- Attended the Generation IV International Forum Project Management Board (GIF PMB) spring meeting held 12 April 2021. Dr. William Windes (Chair of GIF graphite working group) participated, and the PMB was informed that a new graphite research topic on Graphite Decontamination & Decommissioning activities would be discussed at the next GIF Graphite Working Group (GWG) meeting (to be held virtually). With the addition of new GIF members Australia (ANSTO), the United Kingdom (U.K.), and Canada there has been some interest in pursuing this research area.
- Collaborated with Dr. Will Windes and Electric Power Research Institute regarding interest in producing a white paper addressing the need for processing specifications to address the nuclear (irradiation) stability of nuclear graphite grades. The current American Society for Testing and Materials (ASTM) standard (D7219) focuses on unirradiated material property values and does not specify processing traits that produce stable performance under irradiation. Such a white paper would be a good "first step" in introducing key parameters required for a nuclear graphite grade in the future.
- Collaborated, via Zoom on April 22, 2021, among Boise State University (Steve Johns) INL (Will Windes) and ORNL (Anne Campbell), for drafting Nuclear Energy University Program (NEUP) calls for intermediate temperature irradiations of nuclear graphite (300-800°C). Major focuses of NEUP calls will be (a), to support new computational models that accurately describe temperature effects and damage mechanisms, and (b), to support irradiation and post-irradiation examination (PIE) of low dose irradiated nuclear graphite.
- Received all optics and custom-built components for Raman upgrades; the construction of macroRaman spectroscopy is underway.
- Created New record 21-728 to address "HHB technical revisions" for ASME.
- Received ASME Record 20-1307 "Include Carbon-Carbon composites in nonmandatory appendices (as part of Ceramic Matrix Composite material for high temperature reactor (HTR))", ballot comment and review from Working Group- Nonmetallic Design and Materials (WG-NDM) to be addressed.
- Submitted Record 19-2805 on "Eliminate use of fluence and historical dose units and replace with dpa" ballot for ASME BPV III approval.
- Delivered ASME Record 20-1308 on "Modify the Weibull analysis nomenclature and parameter definitions within Subsection section HHA-II-3100 and standardize with ASTM standards for all Nonmetallic Material Core Components" for WG-NDM review.
- Formed the ASME Task Group to address Oxidation issues listed in the NUMARK findings.
- Initiated review of references to nuclear graphite oxidation in the ASME BPVC Section III.5 2019 code. The goal is to find and list those references that need correction or additional clarification to accurately reflect the oxidation behavior of nuclear graphite. A Task Force was formed that will document requested changes and will provide suggestions for replacement.
- Hosted the Weibull workshop for ASME on April 28, 2021. Outcomes included plans to submit a ballot with minor notational changes and to collaborate with Steve Duffy and Eric Baker on developing a method that allows for a quantifiable amount of conservatism in the allowable stress along the same margins as the current method.
- Completed draft report commissioned by ASME on U.K. Damage Tolerance Experience in Graphite Cores and forwarded to William Windes (INL) for review.
- Accepted 13 abstracts for presentation and publication by the Co-Chairs and ASTM conference management (12 previously reported) for the forthcoming ASTM Selected Technical Papers symposium. This event had been linked to the International Nuclear Graphite Specialist Meeting (INGSM) conference scheduled for Chicago in September 2021. With INGSM being re-organized as

a virtual event, the one-day symposium has also been re-organized as a two half-day virtual event immediately before INGSM (23 and 24 September).

- Presented updated slides to the Nuclear Regulatory Commission (NRC) on internal stress modeling in graphite under irradiated conditions.
- Implemented changes to the graphite oxidation model which makes the model more robust and easily coupled to other models in MOOSE.
- Published paper "Probing Basal Planes and Edge Sites in Polygranular Nuclear Graphite by Gas Adsorption: Estimation of Active Surface Area", authors N.C. Gallego. D.J. Arregui-Mena, and C.I. Contescu in the journal Carbon, and available at https://authors.elsevier.com/sd/article/S0008-6223(21)00426-7. The paper presents a new, direct method, based on high resolution gas adsorption measurements, for estimation of basal plane area and active surface area (ASA) of nuclear graphite. The magnitude of active surface area is related to graphite reactivity towards oxidation, fluorination, and tritium chemisorption.
- Began preparation of graphite specimens to be uniformly oxidized for tension strength measurements by the split disc method. First measurements will be done with graphite IG-110 and 2114.
- Captured XCT images of several graphite samples (graphite grades: IG-11, Gilsocarbon, IG-430 and SNG-742). The images will allow us to compare how the porosity network of these grades may influence the thermal conductivity and permeability of graphite. Scans from different samples were acquired to assess and account for the possible microstructural fluctuations in graphite.
- Prepared compression test samples (cylinders 10 mm x 20 mm) of three graphite grades and exposed them to molten FLiNaK salt. The salt intrusion experiments were completed. Samples will be cleaned of any excess salt and compression tested. The results will be compared to that of samples that have not been exposed to molten salt.
- Received acceptance of the conference paper "Recent Advances on Microstructural Characterization and Modeling of Nuclear Graphite" for presentation at American Nuclear Society (ANS).
- Submitted "Porous Random Fields for Nuclear Graphite Elastic Property Predictions" to Carbon. This paper is now under review by this journal.
- Issued the document "Summary of US Department of Energy (DOE) R&D Activities on Graphite Oxidation (2006–2021)" as ORNL/TM-2021/1892, completing the Level 3 ART Milestone M3TG-21OR0501052 on time. This High-Level Deliverable for the Graphite Working Group activity report on oxidation is to be submitted to the PMB of GIF and is now available at https://info.ornl.gov/sites/publications/Files/Pub152182.pdf.
- Completed second cycle of irradiation for High Dose Graphite (HDG)-1 (Total of 123 effective full-power days and 2,460 MWd for the two cycles combined).
- Completed milestone "Complete HDG-1 Irradiation and Support for 1 Advanced Test Reactor (ATR) Cycle in fiscal year (FY) 21", formally completes the INL Advanced Reactor Technologies (ART) Level 2 Milestone (TG-21IN0501021) due July 31, 2021".
- Completed milestone "Complete As-Run Thermal Analysis for the AGC-4 Experiment Irradiated in the ATR, (INL/EXT-21-62386) formally completes the INL ART Level 2 Milestone (M2TG-21IN0501035)", due April 30, 2021.

May

- Completed disassembly of the fourth capsule AGC-4 and re-packaged the graphite samples into the plastic transfer tubes for shipment to the INL Carbon Laboratory. Graphite samples will undergo PIE material property testing and the flux wire samples will undergo dosimetry analysis.
- Completed a subcontract with ORNL to collaborate on developing improved dose estimates for AGC capsule irradiations. The work is intended to improve the dosimetry methodology by irradiating a variety of flux wires within High Flux Isotope Reactor and analyzing the wire activities at ORNL, INL, and other collaborators.
- Attended the second 2021 quarterly meeting of the ASME WG- General Requirements for Graphite and Ceramic Composite Core Components and Assemblies (GR GCCCCA) and WG-NDM, virtually, on May 10th and 11th, 2021 respectively. WG-GR GCCCCA is working on revising tables G-1, G-2 and G-4 in Sec III-A to conform to the new approach of individualized forms. WG-NDM addressed several topics including an ASME inquiry related to allowable data extrapolation, updates on current Task Group items to address the NUMARK report, as well as current ballot status.
- Drafted a report to conclude the ASME inquiry #21-557. The inquiry was discussed in the WG-NDM, Subgroup-high temperature reactor (SG-HTR) and at the BPV III Inquiry Meeting. ASME committee conclusion on inquiry was that limited extrapolation of data is permissible with appropriate justification.
- Elected by voice vote to approve R21-989 on HHB Errata in WG-NDM, SG-HTR and presented at ASME BPV III.
- Discussed issues related to graphite oxidation in the ASME BPVC Section III.5 2019 code during the virtual meeting of ASME graphite working group on May 11, 2021. A Task Group was formed for analyzing the references to graphite oxidation in the current edition (2019) and proposing improvements when necessary. An important mission of the Task Group is drafting white paper(s) on environmental interactions of nuclear graphite in High Temperature Gas Cooled reactor (HTGR) and providing solid documents to inform and support recommended updates to the Code. The Task Group is composed of experts on graphite oxidation behavior, graphite manufacturing, and reactor tolerance to damage from U.S. and U.K.
- Submitted the first complete draft of a White Paper addressing U.K. experience on damage tolerance in graphite cores and implications for new build the ASME Nonmetallics WG for review and comment.
- Coupled the oxidation model previously developed at INL to a finite element analysis stress calculation. This allows for internal stresses to be computed in oxidized graphite.
- Prepared virgin IG-110 transmission electron microscopy (TEM) samples for annealing experiments conducted at 2500°C for 24 hours (i.e. cut-then-annealed TEM samples).
- Received annealed TEM samples back from INL to be characterized at Boise State University.
- Characterized via TEM, IG-110 samples annealed at 2500°C for 24 hours then cut. Examination shows clear evidence of fullerene-like bonding occurring at the edge of crystallites.
- Initiated work for preparation of graphite specimens uniformly oxidized for tension strength measurements by the split disc method. First measurements will be performed with graphite IG-110 and 2114.
- Attended the virtual meeting of ASTM subcommittee D02-F on manufactured carbons and graphite on May 27, 2021. Participants analyzed the status of currently open work items, proposals for new standards, interactions with ASME, and discussed recent voting results.

- Employed XCT segmentations to estimate the open and closed porosity of NBG-18, NBG-17, PCEA, IG-110 and 2114. These segmentations were used to generate artificial uniform oxidation of these microstructures and to predict the effective properties at different levels of oxidation.
- Prepared a presentation with title "Recent Advances on Microstructural Characterization and Modeling of Nuclear Graphite" for the 2021 ANS virtual meeting.
- Presented nuclear graphite technical information at the Canadian Nuclear Safety Commission HTGR Seminar, 3-4 May 2021.

June

- Confirmed that the loaded sample transfer tubes had unexpectedly high gamma ray dose rates varying from 1000 mR/hr to 3000 mR/hr with some variation over the length of the tube. This is at least an order of magnitude higher activity than seen for AGC-1, 2, or 3.
- Performed additional radiological surveys of creep and piggyback specimens in sample transfer tubes to confirm the unexpected high dose rates and eliminate general contamination as a source.
- Performed preliminary non-quantitative gamma spectroscopy on selected sample transfer tubes and non-specimen shuttle pistons. Initial indication on one high activity tube is the presence of cobalt-60 as the isotope responsible for high dose rates. Shuttle pistons did not have sufficient activity to acquire a spectrum in the high background of the HFEF main cell.
- Selected three individual creep samples, one shuttle piston, and one fluence capsule to be transferred to the Materials and Fuels Complex Analytical Laboratory for quantitative gamma spectroscopy.
- Submitted draft AGC-4 Disassembly report for review.
- Evaluated dose dependency of oxidation and drafted memo regarding the status of irradiated graphite oxidation. NBG-25 split specimens from AGC-1 show approximately 10% increase in oxidation rate for each 1 dpa up to 6.8 dpa relative to unirradiated companion split specimens.
- Commenced draft of peer-reviewed manuscript on the microscopic response of thermally annealed nuclear graphite.
- Prepared TEM specimens of IG-110 nuclear graphite to electron transparency via oxidative techniques and sent to INL for thermal annealing to support peer-reviewed manuscript.
- Conducted Stopping Range of Ions in Matter calculations using experimental parameters of ion milling nuclear graphite IG-110 to electron transparency to support peer-reviewed manuscript.
- Annealed creep specimens of IG-110 thermally at 2500°C for 81 hrs., held at a compressive load of 265 lbs. and prepared to electron transparency via ion milling.
- Conducted preliminary analysis of creep specimens via TEM.
- Circulated recently developed draft white paper on damage tolerance in graphite cores of UK reactors and its implications for new builds for comment to ASME Nonmetallic Working Group members.
- Completed construction of macroRaman spectrometer and measured standard specimens (graphite, silicon).
- Measured thermal diffusivities of graphite samples (HOPG, IG-110, PCEA) using photothermal radiometry.
- Presented ASME code rules and ASTM standards integration for ceramic composite core materials and components at the HTR2021 conference on June 3rd, 2021. Apart, from discussing the code approach and the standards developed, it provided background on the application as well as the type composite material provisioned for nuclear use.

- Sent document NTB-4-2021 titled “Background Information for Addressing Adequacy or Optimization of ASME BPVC Section III, Division 5 Rules for Nonmetallic Core Components” for publishing after completion of ASME copyediting, and formatting.
- Reviewed for first ballot proposals with the intention to submit records R20-1308 on nomenclature as well as 2-parameter Weibull changes, R20-1306 on abrasion and erosion as well as new proposed record on addressing oxidation issues as it relates to graphite-moderated HTRs. Moreover, action on the revision of the Companion Guide of ASME BPVC Sec III.5 was received and will be addressed for the upcoming virtual code week, scheduled for the week July 25-30, 2021.
- Identified a few places in ASME BPVC Section III.5 which are either incorrect or not applicable to graphite-moderated HTRs (specifically, HTGRs and Molten Salt Reactors (MSRs)). The Task Group on graphite oxidation provided a list of obvious changes to be discussed and balloted at the coming July 2021 meeting of Non-Metallic WG. The changes include dropping references to radiolytic oxidation and oxidation by hydrogen; adding carbon dioxide as possible oxidizing impurity in helium coolant; and emphasizing that graphite oxidation must be treated as a localized process and its density profile must be known for stress analysis.
- Participated in an ad-hoc virtual meeting of ASTM D02.F0 Subcommittee held on June 16, 2021. The ad-hoc meeting was held to complete analysis of work items that could not be discussed at the regular virtual meeting of May 27, 2021.
- Completed first draft of a new paper covering the topic of modeling nuclear graphite oxidation in the kinetic regime. The paper combines experimental oxidation testing (following ASTM 7542), a 3D random pore model, XCT, and other characterization methods to demonstrate the microstructural and kinetic basis for the large difference in oxidation mass loss between IG-110, PCEA, and NBG-18. The team will continue the internal review process and plan to submit to journal in the near future.
- Continued planning to initiate a screening study for uniform oxidation of split disc samples (adhering to ASTM D8289). The planning has included feasibility of XCT to demonstrate uniformity of oxidation as well as simulation of oxidation to compare with experiments.
- Combined in-situ thermal annealing experiments and TEM imaging of graphite samples to compare the effects of temperature on thermal cracks and round pores. The results demonstrate that thermal cracks close at a higher rate than gas-evolution porosity.
- Conducted Raman spectroscopy experiments on as-received and neutron irradiated fractured surfaces of POCO AXF-5Q graphite. These results will help to understand the neutron irradiation effects of binderless graphites.
- Completed report titled “Initial Developments in Modeling Graphite Behavior,” fulfilling ART Level 3 Milestone (M3TG-21IN0501037), due June 30, 2021.
- Completed ART Level 3 Milestone (M3TG-21-IN05010310), “Issue Baseline Data Status Update Memorandum,” due June 30, 2021.

1.4 Methods

Highlights of methods activities during April, May and June 2021 are as follows:

April

- Attended the first benchmark meeting on April 30, 2021 with Canadian Nuclear Laboratories, Argonne National Laboratory and Oregon State University (CNL/ANL/OSU) to evaluate possible future collaborations on High Temperature Test Facility (HTTF) modeling and benchmarks. All parties are interested and have funding to participate in the benchmark.

- Approval has been received for the abstract on HTTF PG-27 using Reactor Excursions and Leak Analysis Program (RELAP5)-3D from the NURETH conference. The full paper will be submitted in June.
- Following previous test scenario DataQuality066, where steady-state operating conditions could not be met during the scheduled shift times of the operators and the test was prematurely concluded, adjustments were made to the test start times and personnel shift periods to allow an extended duration testing window. The steam outflow test was repeated a second time during DataQuality067. This attempt was successful in meeting the required acceptance criteria and allowed the facility to achieve a new steady-state operation with the higher system pressures induced by the restricted steam outflow. The impacts on the facility suggest a mild effect on stability, however it was not as profound as the case where we restricted the inlet. Additional levels of steam outlet restriction are slated to be examined in upcoming testing.
- In anticipation of a scheduled power outage to switch high voltage equipment on co-located facilities, the Natural Convection Shutdown Heat-Removal Test Facility (NSTF) team postponed their next planned test and instead shifted their attention to continued post-processing of experimental data and upkeep of the program Quality Assurance records. Additionally, though testing is scheduled to continue until the September timeframe, planning efforts began on a facility maintenance period scheduled to begin early FY22. This shutdown, anticipated to extend 4-months, will be used to repair the faulted Guard heaters, examine the cavity interior, and collect emissivity measurements of the test section and heated surfaces.

May

- Completed preparations for the final case of the restricted steam outlet parametric to examine the influence of two-phase operation at systems pressures of approximately two atmospheres.
- Successfully completed DataQuality068 late in the reporting period, and established the highest system pressures observed to date, peaking at just below two atmospheres within the gas space of the primary tank. In addition to completing the last (planned) test case within the steam outflow parametric series, this scenario was extremely insightful in understanding the instability mechanisms and re-stabilization conditions for the test loop.
- Completed housekeeping and laboratory maintenance, including replacement of the facilities resin bed deionized water tanks, generation of a new batch of deionized water, and installation of a dedicated uninterruptible power supply for network gear to increase operational reliability during power dips or brownouts.

June

- Full paper “Sensitivity Analysis And Relap5-3D Simulation of Pressurized Conduction Cool Down Phenomena at the High Temperature Test Facility” submitted to NURETH 2021.
- Follow-up meetings on the planed HTTF benchmark have been held. INL/ANL/CNL/OSU started looking into the HTTF data and selected a few tests to be modeled as part of the benchmark. Preliminary work on the benchmark specification has been started.
- Draft of the DOE FY21 milestone “RELAP5-3D simulation of PG-27 test at the HTTF facility” has been submitted for review.
- DataQuality069, an extended duration boil-off test, was conducted and successfully completed by the experimental team. Due to large voiding in the chimney region, swelling of this hot leg allowed the loop to flow continuously even as the level within the tank fell 35-inches below the chimney inlet, with only approximately 20% of the tank inventory remaining.

- Members of the NSTF team presented at the ANS Annual Conference (virtual), sharing latest results from experimental, modeling, and quality assurance activities within the parent program.

2. SIGNIFICANT ACCOMPLISHMENTS

2.1 Fuels Development and Qualification

2.1.1 Completion of a Report on Fission Product Concentration Profiles in AGR-3/4 Rings at INL

A report summarizing all the data from destructive "sampling" of AGR-3/4 graphite and graphitic matrix rings was completed and issued. (Stempien, John D. 2021. "Measurement of Fission Product Concentration Profiles in AGR-3/4 TRISO Fuel Graphitic Matrix and Nuclear Graphites." INL/EXT-21-62863. Idaho National Laboratory.)

This report provides all the measured fission product concentration profiles for all sampled rings, a detailed uncertainty analysis, a discussion of the potential for cross contamination, and tables of all the data that can be used in ongoing attempts to derive new fission product diffusivities. Excerpts from this report are given below for AGR-3/4 Capsule 12, the most recent rings that were sampled. The conclusions from the report are also excerpted.

2.1.1.1 Capsule 12 Inner and Outer Ring Fission Product Profiles

Figure 1 and Figure 2 give the radial profiles of select fission product concentrations for the inner ring (IR) and outer ring (OR) at the axial center and bottom of the rings, respectively. Appendix B (not excerpted into this quarterly report) features tabularized summaries of the fission product concentrations, ring segment volumes, and uncertainties. The IR was made of graphitic matrix, and the OR was made of PCEA graphite. The nubs on the outside of the OR were milled and collected separately from the radial segments. In the as-fabricated condition, the gap between the IR and OR was 0.089 mm, and the PIE measurements showed the gap increased to 0.14 mm at the EOI (Stempien et al. 2016). The average compact-to-IR gap increased from 0.069 mm to 0.10 mm over the course of the irradiation.

Because the equipment had not been used for about one year, some additional clean, unirradiated graphite was milled at various points before and after the Capsule 12 milling activities. This served to further sweep out the cyclone separator and was used as practice for the hot cell technicians to refamiliarize themselves with the sampling processes. Prior to taking the first samples on the bottom end of the Capsule 12 IR, a vial of clean graphite fines was placed at the outlet from the cyclone separator, and the cyclone separator was run for five minutes. Then, the usual pre-sampling activity was performed by milling about one gram of clean, unirradiated graphite and collecting it in the cyclone separator. After completing milling of the Capsule 12 IR (and before beginning milling of the OR), the usual three post-sampling cuts of clean graphite were performed, followed by an additional three clean graphite samples. Then, two pre-sampling activities involving milling and collecting clean graphite (instead of the usual one) were performed prior beginning sampling of the bottom end of the OR.

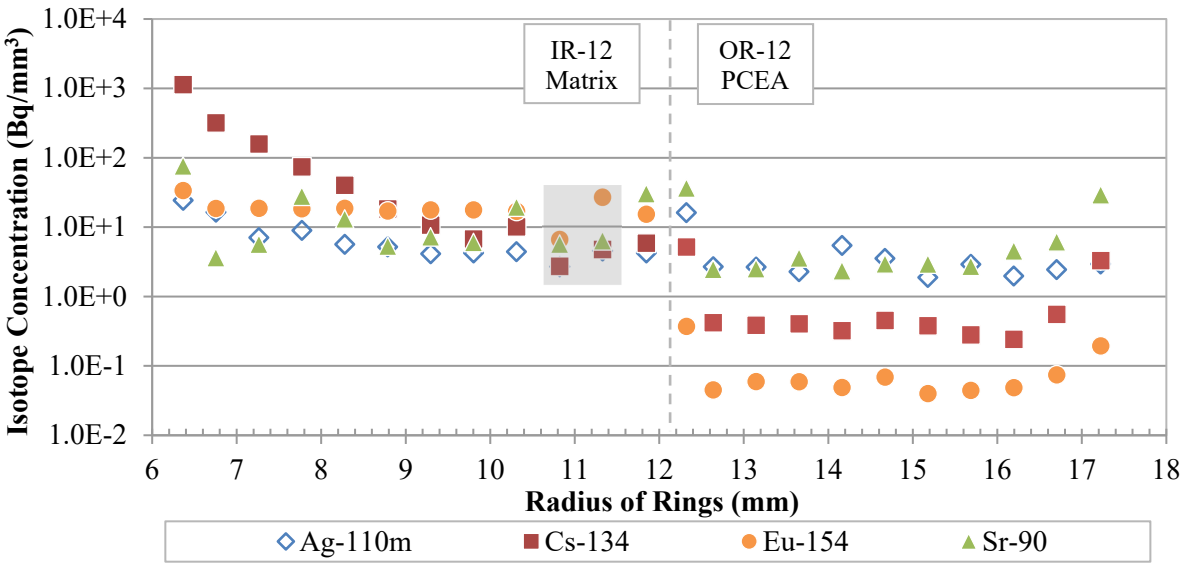

Figure 1. Radial profiles for select fission products at the axial center of the Capsule 12 IR and OR.The open symbols denote values derived from minimum detectable activities. Gray shading shows the IR-12 segments where roughly 60% of the third segment (around x = 10.8 mm) was collected in the vial for the second segment (around x = 11.4 mm).

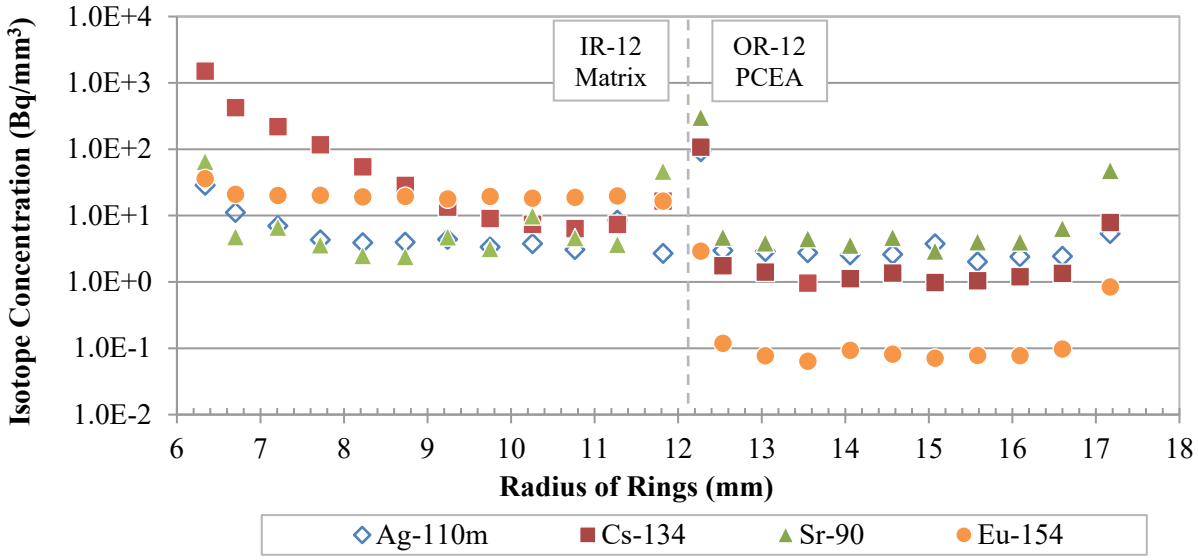

Figure 2. Radial profiles for select fission products at the axial bottom of the Capsule 12 IR and OR. The open symbols denote values derived from minimum detectable activities.

2.1.1.2 Conclusions

Radial fission product concentration profiles were measured for gamma-emitting fission products (e.g., Ag-110m, Cs-134, and Eu-154) and beta-emitting Sr-90 in the inner and outer carbon rings from six different AGR-3/4 irradiation capsules. Two of the IRs were PCEA graphite. Three of the IRs were graphitic matrix material similar to the historic German A3-27 matrix formulation. One of the IRs was IG-110 graphite. Five of the ORs were PCEA graphite, and one of the ORs was IG-110 graphite. In future work, these profiles will be compared in detail to simulations of AGR-3/4 fission product transport and to non-destructive measurements. The ultimate goal of this work is the extraction of new fission product transport parameters (e.g., diffusivity) from these data. The immediate conclusions are as follows:

- Elevated concentrations of Ag, Cs, Eu, and Sr were detected on the outer surfaces of some IRs and ORs. This indicates a short-circuit pathway may exist whereby gas-phase fission product transport occurred in the gaps between the compacts and the IR and the IR and OR. This complicates the analysis because it means that one-dimensional diffusive transport was not the only transport mechanism.
- Ag-110m profiles had the most variation. Some profiles were peaked at an inner or outer surface. Some were peaked at the middle of the ring wall thickness. Some went through inflection points. Some increased radially outward. Some decreased radially outward. In some instances, the concentrations varied significantly depending on whether the ring was sampled at the axial center or at one of the ends. The axial non-uniformities are generally consistent with observations in non-destructive gamma scanning of the rings, which also showed non-uniform axial distributions for Ag-110m. This may adversely impact the ability to extract reasonable diffusion coefficients for this isotope.
- In many cases, the IR Cs-134 profiles decrease somewhat linearly from the inside to the outside, and the qualitative shape of these profiles compared reasonably with the model. The step changes in concentration across the IR-OR gap were generally consistent with the model predictions as well. The ORs tend to have flatter Cs-134 profiles, but there are also OR profiles (particularly in the hotter capsules) that decrease noticeably in the outward radial direction. Local increases in concentration at the OR's inner and outer surfaces are more pronounced than for the IRs. This combined with the flatter, though in some cases still linear, profiles in the ORs suggest that some effect (i.e., gap transport) in addition to simple diffusion is taking place.
- Eu-154 and Sr-90 profiles tend to have very similar shapes. This suggests that they transport via the same mechanisms and have the same rate-limiting steps. In the IRs, both isotopes have their highest concentrations at the inner surface and drop sharply moving radially outward where they are relatively flat across the rest of the IR. This indicates a transport process where the isotopes are sorbed on the inner surface of the ring, but diffusion into the ring from that surface is quite slow. By comparison, the OR profiles are largely flat and feature maxima at the inner and/or outer surfaces of the OR. There are frequently local maxima at IR outer surfaces as well. These local maxima on the outer surfaces could indicate that gap transport has a minor, but noticeable, effect. In some capsules, the qualitative Sr-90 behavior across the ring gaps was consistent with the model (using legacy Sr-90 transport parameters), but in other capsules, the model was inconsistent with the measurements and seemed to underestimate the amount of Sr-90 in the ORs.

- The analysis of the small nubs on the outer surfaces of some of the ORs revealed fission product concentrations in the nubs that were often higher than in the outermost segments of the rings. This supports the hypothesis that short-circuit, gap transport occurred, causing relatively high surface concentrations on the outer surfaces of the rings. Comparing the ratios of the fission product concentrations in the nubs to those in the outermost segment of the ORs suggests that gap transport was less significant at high temperatures where diffusive transport was rapid enough to clearly overpower gas-phase gap transport and more significant at lower irradiation temperatures in the cooler capsules, where diffusive, solid-state transport is not as rapid.
- Some Sr-90 transport via a gaseous precursor (Kr-90) and a highly volatile intermediate (Rb-90) likely occurred in all capsules. This was most noticeable in the hottest capsule, Capsule 7, which was the only capsule where the Sr-90 concentration was higher in the nubs than in the OR segment; while at the same time, the other isotopes concentrations were lower in the nubs than in the OR segment. However, the distinct similarities in the shapes of the Eu-154 and Sr-90 profiles across rings in all capsules suggests that the dominant mechanism of Sr-90 transport is similar to that of Eu-154 and that the transport of short-lived Sr-90 precursors is not a major effect.
- Total Sr-90 inventories were estimated in the rings based on the results from the physical sampling. These results will be used to adjust the predicted particle and/or compact releases used in the AGR-3/4 fission product transport model.

Given the different irradiation temperatures among the capsules and the rings, it was not possible to discern fundamental differences in the transport of isotopes within the different carbon materials (i.e., graphitic matrix, IG-110, or PCEA). It may be possible to do this while determining diffusion coefficients from the concentration profiles. Future work will also rigorously compare the model predictions with the measured concentration profiles.

2.1.2 Completed Exterior Visual Exams, PGS, and Neutron Radiography of Capsules 1 and 2 from AGR-5/6/7 at INL

As of the end of June 2021, the work completed on Segment 1 (which contains Capsules 1 and 2) is sufficient to fulfill a Level 2 milestone. The paperwork announcing completion of the milestone will be filed in July 2021.

Segment 1 was moved into the main hot cell at HFEF, and it was suspended vertically using a special fixture. Photographs were taken along the length of the test train and at four rotations 90 degrees apart. Figure 3 shows a montage of a set of photographs of the test train taken through the hot cell window. Welds visible on the exterior of the test train denote the interfaces between different capsules. No unusual discoloration or damage to the test train was observed.

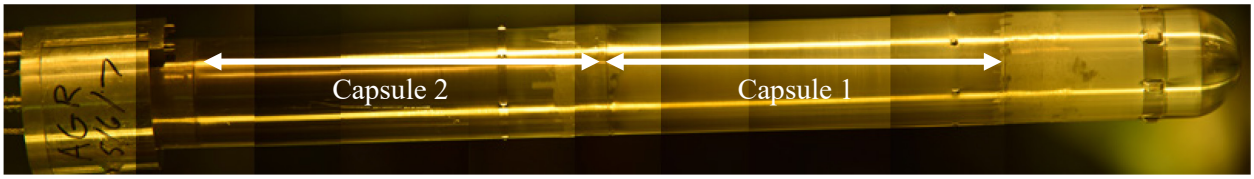

Figure 3. Montage of photos of Segment 1 of the AGR-5/6/7 test train taken through the hot cell window. Lighting in the hot cell was not uniform. Striations are artifacts from combining multiple photos taken at different locations with different lighting along the test train.

Next, the test train was moved to the part of the hot cell that houses the PGS. The gamma detector system consists of a digital multichannel analyzer and a high-purity germanium (HPGe) detector that is surrounded by a Compton suppression detector. The collimator is approximately 2.13 m long with an aperture that has a fixed width of 2.22 cm and a variable height of 0.254 to 0.00254 cm. A stage suspends items before the collimator and moves them in a plane parallel to the face of the collimator. The stage can

also rotate items about a central axis. AGR-5/6/7 Segment 1 was suspended from the PGS stage by the same fixture used for visual exams. The segment was then scanned from top to bottom, once on the side to the left of its radial center and once on the right side.

Figure 4 shows the total gamma count rate (in units of counts per second) from along the left side of the test train. The right-side scans were virtually identical. Areas of high gamma count rates indicate the presence of substantial Co-60 from neutron activation of the stainless-steel test train capsule head and floor pieces. Within a capsule, the total gamma count rate drops from top to bottom due to lower burnup in the fuel and less activation of the stainless steel in accordance with the neutron flux shape in ATR. AGR-5/6/7 compacts were stacked on top of each other, and each capsule contained multiple stacks of compacts. In Capsule 1, for example, there were ten stacks of nine compacts. Small, regularly spaced dips in the gamma count rate indicate where two compacts are in contact. In Figure 4, Compact levels 1, 5, and 9 are highlighted for Capsule 1. Capsule 2 had eight compacts in four stacks, and compact levels 1, 4, and 8 are highlighted in Figure 4. There are no indications that fuel or interior components of the capsules had relocated or were out of position.

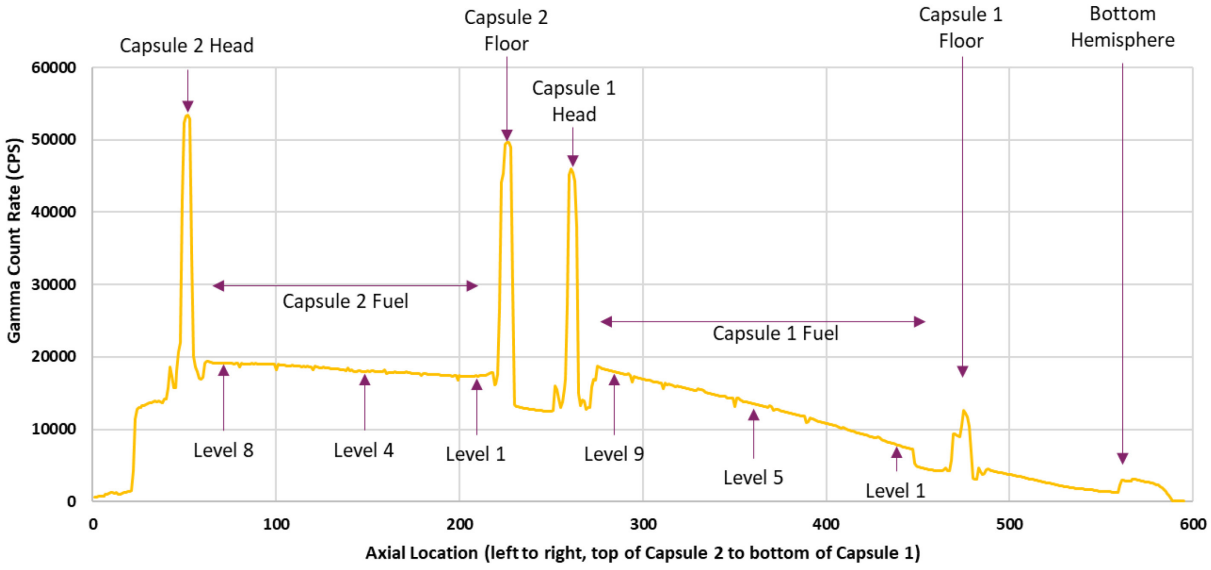

Figure 4. Total gamma count rate detected via PGS along the length of Segment 1 of the AGR-5/6/7 test train.

Segment 1 of the test train was examined by neutron radiography at the Neutron Radiography reactor at HFEF. The test train was suspended in front of a neutron beam line and indium and dysprosium films behind the test train registered transmitted epithermal and thermal neutrons, respectively. Figure 5 shows thermal and epithermal neutron radiographs of AGR-5/6/7 Capsule 1 taken at two orientations 90° apart. Figure 6 shows a montage of thermal neutron radiographs adjusted to make each of the nine layers of compacts more easily visible. The same kind of detail was observed in Capsule 2.

Equipment to disassemble Capsules 1 and 2 and recover the fuel compacts and capsule internals has been constructed and has completed Phase I and Phase II qualifications. Following in-cell Phase III qualification, the capsules will be opened, and additional PIE will begin.

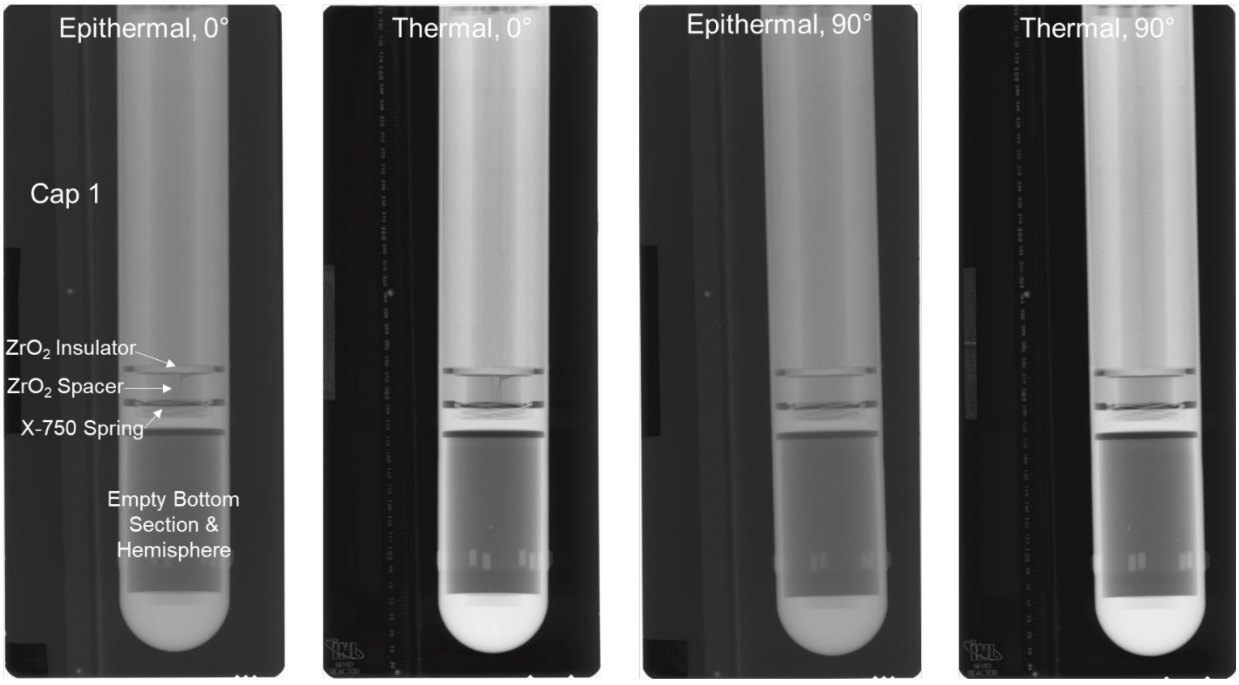

Figure 5. Thermal and epithermal neutron radiographs of AGR-5/6/7 Capsule 1 taken at two orientations 90° apart.

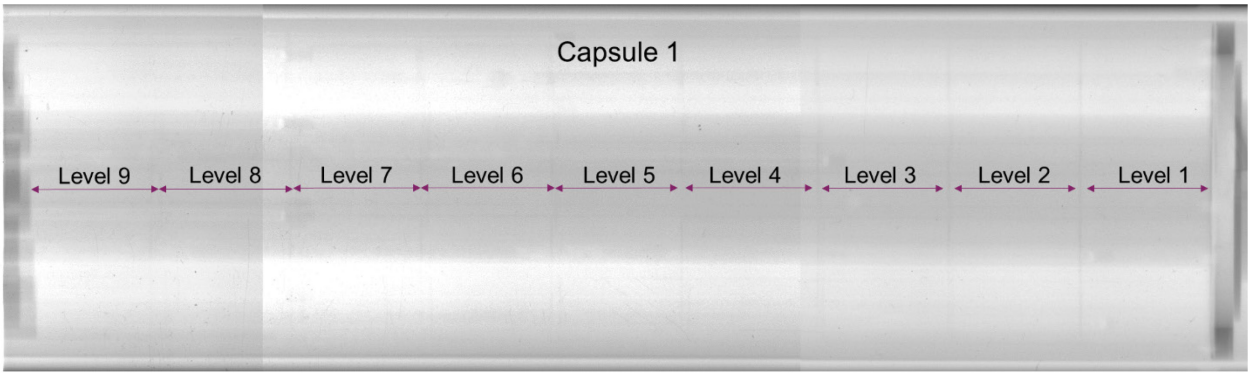

Figure 6. Montage of cropped thermal neutron radiographs adjusted for brightness and contrast to better show the individual levels of compacts in Capsule 1.

For More Information:

John D. Stempien (john.stempien@inl.gov)
John D. Hunn (hunnjd@ornl.gov)
Tyler J. Gerczak (gerczaktj@ornl.gov)
Grant W. Helmreich (helmreichgw@ornl.gov)

2.2 High-Temperature Materials

This quarter, INL staff continued to support ASME BPVC Section III, Division 5 Committee activities. This support included attending and participating in various committee meetings held as part of the May Code Week which was held virtually. During this Code Week, updates on ongoing work at INL were provided. This included an update to the committee on Allowable Stress Criteria regarding an upcoming ballot on the tertiary creep-based criterion. In addition to attending committee meetings that

occur during Code Week, an INL staff member has been participating in the Powder Metallurgy Hot Isostatic Pressing process group which meets monthly. This process group reports to the Section III, Division 1 Advanced Manufacturing Task Group. INL staff also attended and participated in the Office of Nuclear Reactor Deployment Advanced Materials R&D program review this quarter. This participation included giving a presentation titled “Notch Effect Testing and A800H Weldment.”

Various creep-rupture tests of notched Alloy 617 continued to be sustained this quarter. Tests with U- and V-notches are being conducted. The following four paragraphs provide an update on this testing.

The U-notch geometry is also referred to as a Bridgemean notch. This geometry enables the impact of a multiaxial stress state to be investigated. Modifying the radius of the U-notch alters the multiaxial stress state. For this study, specimens with small- or large-radius U-notches were machined so that two different multiaxial stress states could be investigated. There are two small-radius base-metal U-notch creep-rupture tests that are in progress. These tests are being conducted at different temperatures and initial applied stresses and have been running for over 15,000 hours.

The V-notch geometry enables the notch behavior of a material to be qualitatively evaluated as strengthening or weaking for a given temperature and stress. The specimen is comprised of a V-notch and straight gauge with the same minimum diameter. A material is notch weakening if rupture occurs in the notch and strengthening if rupture occurs in the straight-gauge. All completed V-notch creep-rupture tests have been notch strengthening. These tests have had rupture lives ranging from approximately 500 to 3,000 hours. Notch behavior is sensitive to variations in temperature and stress. This leads to concerns that the notch behavior may transition from strengthening to weakening at test conditions more realistic of service conditions. Consequently, V-notch creep-rupture tests with an estimated rupture life of 8,000 and 100,000 hours are in progress. However, it is unrealistic to wait 100,000 hours to learn the outcome of a test. Therefore, XCT is being utilized to periodically, nondestructively characterize the specimens with a 100,000-hour estimated rupture life. The goal of the XCT characterization is to identify the failure location prior to rupture. The two tests with a 100,000-hour estimated rupture life were interrupted this quarter for XCT characterization. This interruption occurred approximately 28,812 and 21,739 hours into the test for the base- and weld-metal specimen, respectively. XCT data was collected and analyzed for both of these specimens. The results are shown in Figure 7 and Figure 8. The base metal test was reloaded and restarted. Unfortunately, there was an issue with the test restart for the weld-metal specimen that resulted in the test being aborted. A new weld metal V-notch creep-rupture test was started that is being conducted at the same temperature and initial applied stress as the aborted test. Prior to testing, this specimen was characterized with XCT.

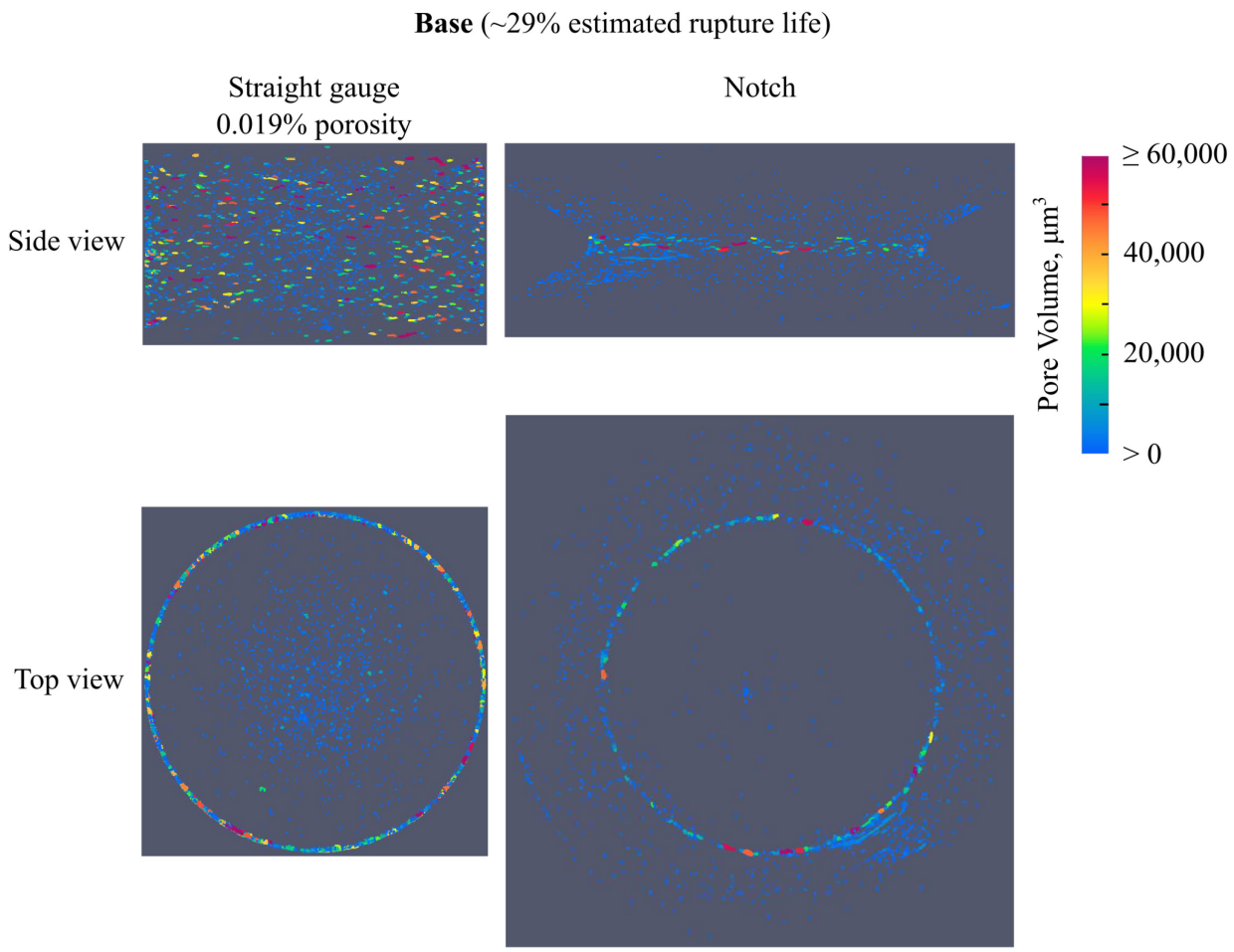

Figure 7. A side and top view of the creep damage characterized by XCT in the straight gauge and notch of a base-metal V-notch specimen. The specimen was interrupted approximately 28,812 hours into an 800°C creep-rupture test with an initial applied stress of 35 MPa.

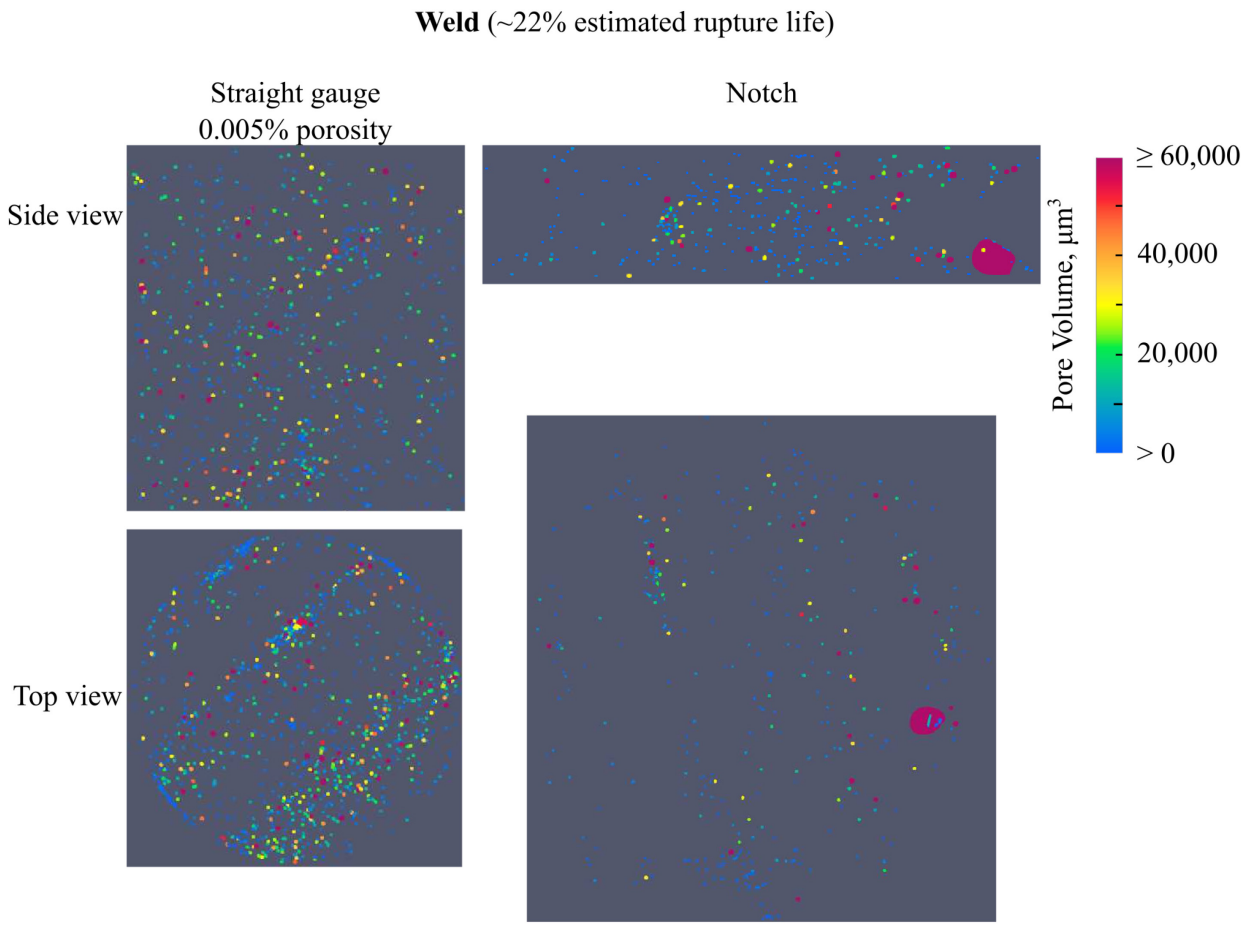

Figure 8. A side and top view of the creep damage characterized by XCT in the straight gauge and notch of a weld-metal V-notch specimen. The specimen was interrupted approximately 21,739 hours into an 800°C creep-rupture test with an initial applied stress of 35 MPa.

In order to interpret the XCT data being collected from the long-term V-notch creep-rupture tests, the relationship between creep damage and rupture life needs to be understood. This necessitates periodically collecting XCT data from V-notch creep-rupture tests with shorter rupture lives. This quarter some of the XCT data collected from these tests were analyzed. A base-metal V-notch specimen that was tested at 800°C with an initial applied stress of 65.3 MPa is shown in Figure 9 and Figure 10. This specimen was characterized with XCT at 71%, 89%, and 100% life. Rupture occurred in the straight gauge. From Figure 9, it is apparent that as the test progressed, the number and size of the cavities increased. No cavities larger than the resolution of the XCT were detected in the notch at 71% and 89% life. Figure 10 shows the creep damage in the notch and straight gauge after rupture. Damage in the notch was primarily limited to the surface at the notch tip. An intermediate weld-metal V-notch test with an estimated rupture life of 8,000 hours is ongoing. The test has been interrupted at 13% and 25% life. The results are shown in Figure 11.

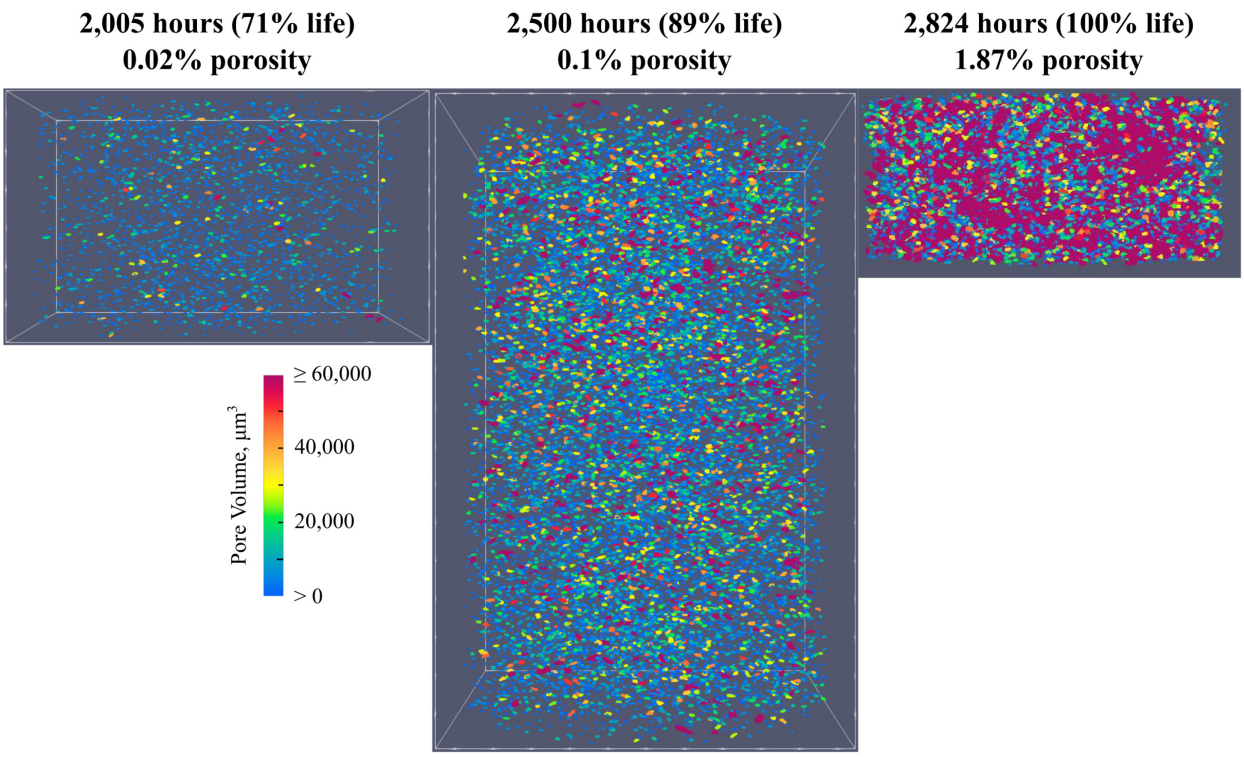

Figure 9. Creep damage characterized using XCT in the straight gauge of a base-metal Alloy 617 V-notch creep-rupture specimen at 71%, 89%, and 100% life. The test was conducted at 800°C with an initial applied stress of 65.3 MPa.

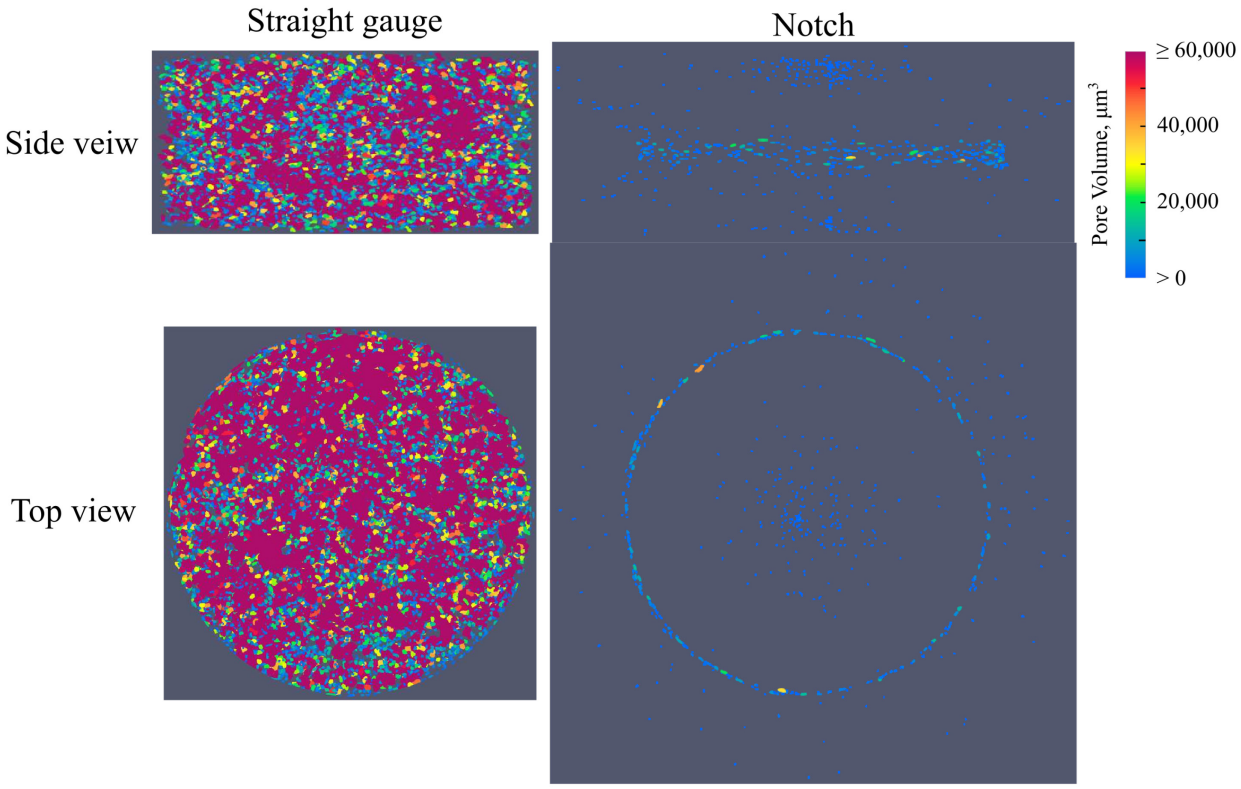

Figure 10. Creep damage characterized using XCT in the straight gauge and notch of a base-metal Alloy 617 V-notch creep-rupture specimen after rupture in the straight gauge. The test was conducted at 800°C with an initial applied stress of 65.3 MPa.

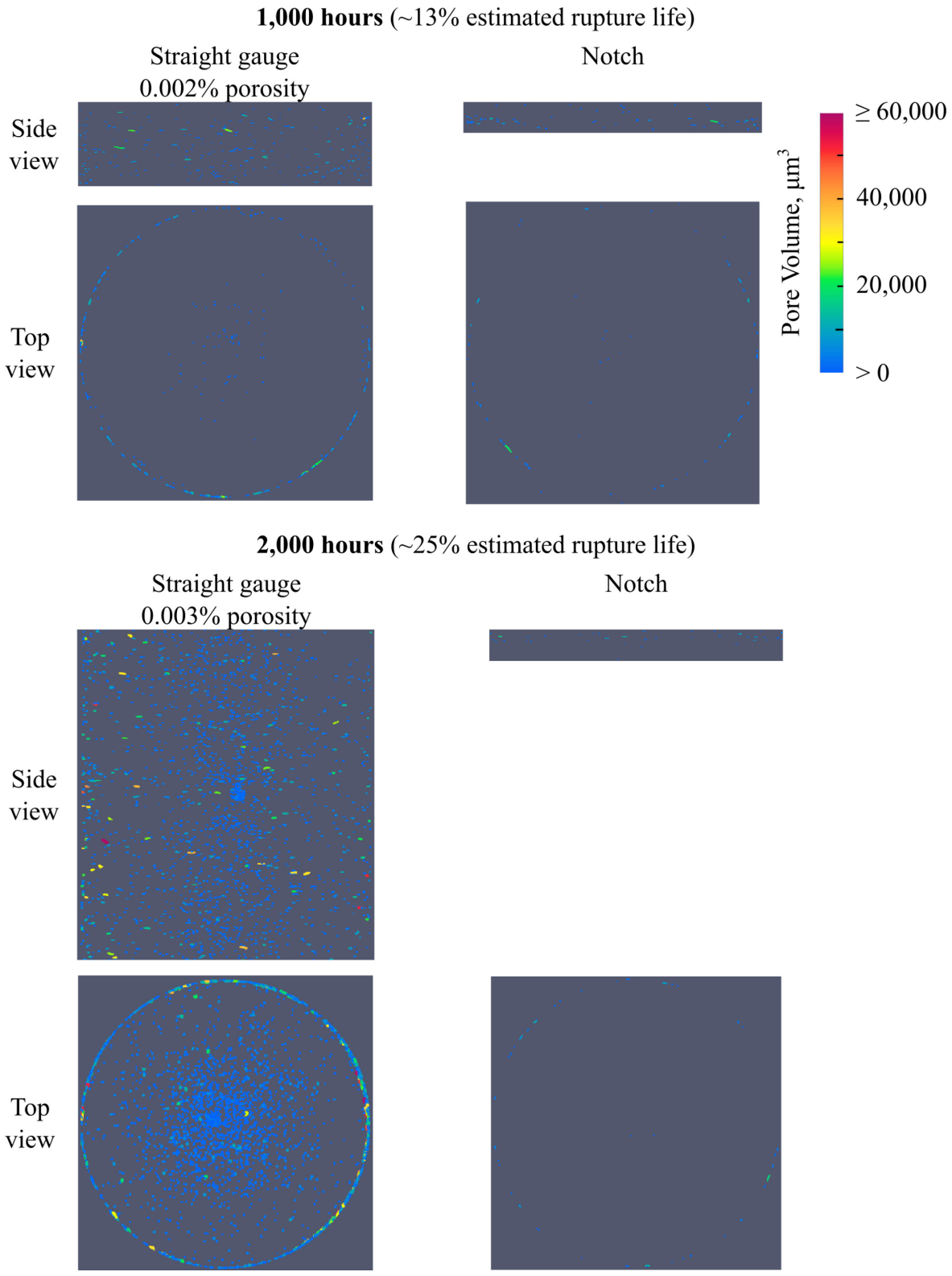

Figure 11. Creep damage characterized using XCT in the straight gauge and notch of a base-metal Alloy 617 V-notch creep-rupture specimen. The test is being conducted at 800°C with an initial applied stress of 60 MPa. The test has been interrupted at 13% and 25% of the estimated life.

There are several limitations to the V-notch specimen geometry. One is that the results from these tests are strictly qualitative. No quantitative information regarding the extent of the notch strengthening or weakening behavior is learned. Furthermore, to date, only minimal creep damage has been observed in the V-notch. This has precluded an understanding of the relationship between cavitation damage and rupture life in the V-notch. Consequently, a specimen comprised of two V-notches is in the process of being tested uninterrupted to failure.

Work to revivify the test capability to investigate the impact of environment on fatigue properties and crack growth is ongoing. This quarter, feedback issues in the test system were corrected. No major issues were detected during a test conducted in air to verify the crack growth experimental setup. Alloy 617 specimens are in the process of being machined.

Creep-fatigue of weldment testing is being conducted to assess the adequacy of the requirements in Section III, Division 5 of the ASME BPVC regarding the creep-fatigue of weldments. To date, the experiments have been conducted with the weld centered with respect to the extensometer and reduced section. This quarter, it was determined that the primary crack occurred in the weld metal for the seven specimens that were characterized with optical microscopy. At least one specimen for each test condition conducted was characterized.

Work has been ongoing to identify a filler metal for Alloy 800H with improved stress rupture factor (SRF) values compared to the SRF values for the filler metals qualified in Section III, Division 5 of the ASME BPVC. An overmatched filler metal, Alloy 617, was investigated. Preliminary results do not indicate that Alloy 617 will significantly improve the SRF values. A report on these findings was drafted this quarter. A research and development program is in progress to investigate a matching filler metal UTP A 2133 Mn. This quarter, UTP 2133 Mn was procured. Efforts are ongoing to setup a subcontract with a consultant based in the Netherlands to leverage his industry expertise with this matching filler metal.

For More Information:
Sam Sham (tingleung.sham@inl.gov)
Richard Wright (richard.wrightt@inl.gov)
Michael McMurtrey (michael.mcmurtrey@inl.gov)
Joseph L. Bass (joseph.bass@inl.gov)
Ryann Rupp (ryann.rupp@inl.gov)

2.3 Graphite Development and Qualification

2.3.1 Irradiation Experiments–Graphite

2.3.1.1 AGC-4 Disassembly and PIE

Disassembly and transport of the AGC-4 experiment have been encumbered by mechanical challenges and by higher than expected radiological activity. Ultimately, milling operations were successful for the removal of recalcitrant center stack piggyback samples as indicated in Figure 12 and Figure 13. Additional analysis and consideration continue in pursuit of mitigation strategies to enable transport and safe handling for PIE.

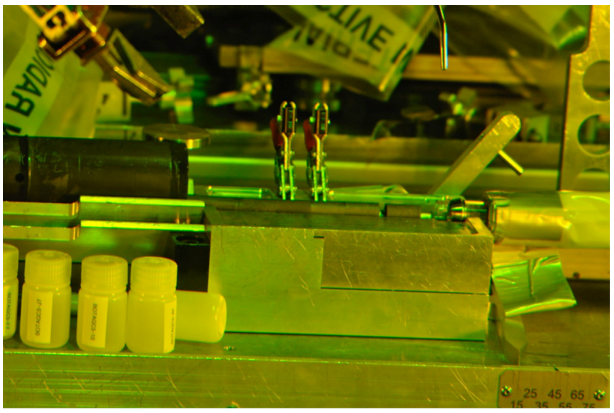

Figure 12. Removal and packaging of creep and un-stressed AGC-4 graphite samples from the graphite body in preparation for survey and transport.

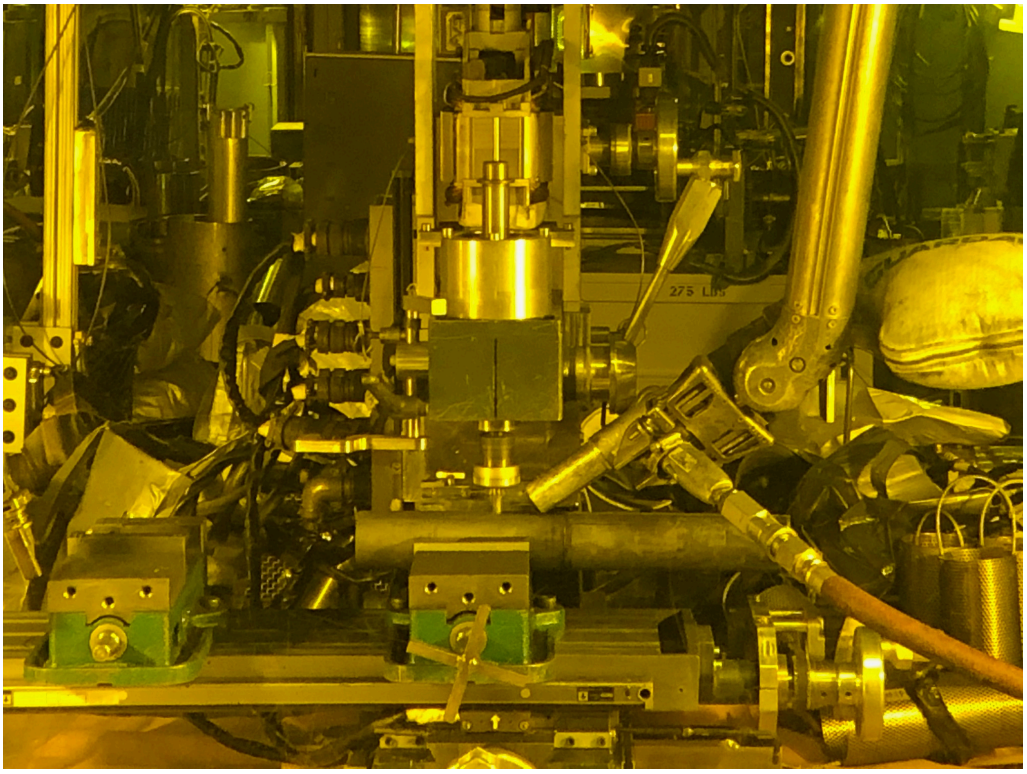

Figure 13. Using HFEF Main Cell milling machine to segment AGC-4 graphite body to free piggyback samples from center channel.

2.3.1.2 Oxidation of Irradiated Graphite

The dose dependency of the oxidation rate effect, previously observed for NBG-25 graphite between 600°C and 700°C (for the narrow dose range, nominal 6.5 dpa dose), was explored for a range of irradiation doses at the single oxidation temperature of 650°C. Continuing the oxidation testing of the NBG-25 grade, AGC-1 button specimens and unirradiated companions (nominally 0.5-inch in diameter by 0.25 inch) were split into four pieces allowing four oxidation rate tests for each dose indicated. The log of the mass normalized oxidation rate is shown plotted with increasing dose in Figure 14. In the left image of Figure 14, the widespread in even the unirradiated oxidation rate results suggest that the splitting process may contribute to scatter in the oxidation data. However, averaging the oxidation rates for split

pieces of the same dose history as in the image at the right in Figure 14, suggests a more consistent trend. The overall effect of irradiation approximately increases the oxidation rate of NBG-25 by about 10% for each 1 dpa of dose exposure.

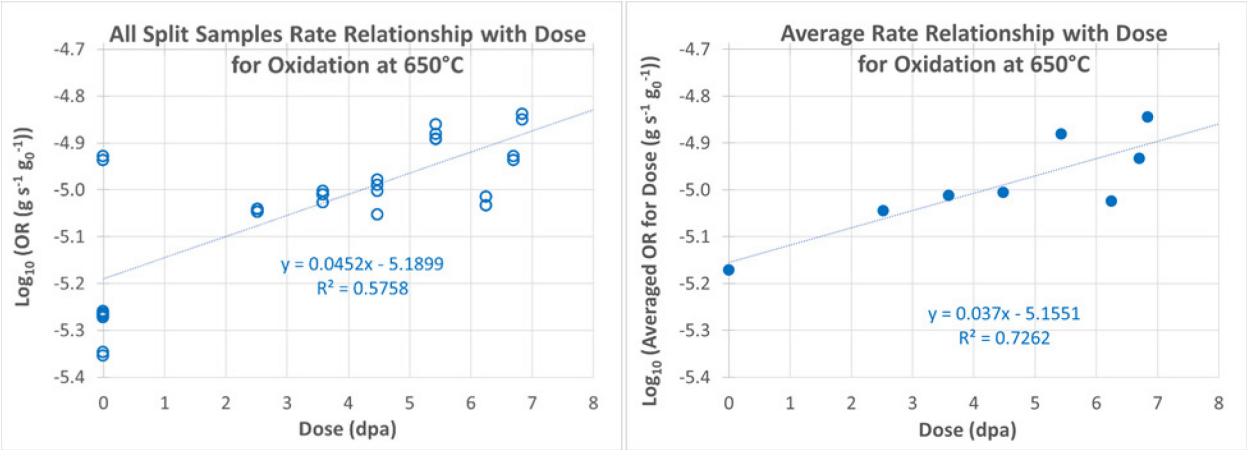

Figure 14. Dose dependency trend in oxidation of NBG-25 at 650C: data as measured for all tests (left) and average of data for each irradiation condition (right).

2.3.2 Baseline Characterization

2.3.2.1 Microstructural Studies: Pore Morphology Analysis via Transmission Electron Microscopy (TEM) During In-situ Thermal Treatment

In-situ thermal treatment experiments were performed on TEM lamella to study the effects of temperature on different pore morphologies. TEM lamellas were mounted in a Nuclear Science Users Facility microelectromechanical system-based heating holder for temperature treatment. High resolution TEM micrographs were taken from thermal cracks and gas evolution porosity to compare the crack or pore closure as a function of temperature. The results showed that thermal cracks are more prompt to earlier closure due to temperature changes and they also exhibit a more pronounced shape change when compared to gas evolution porosity. The evolution of the studied thermal crack as a function of temperature is shown in Figure 15.

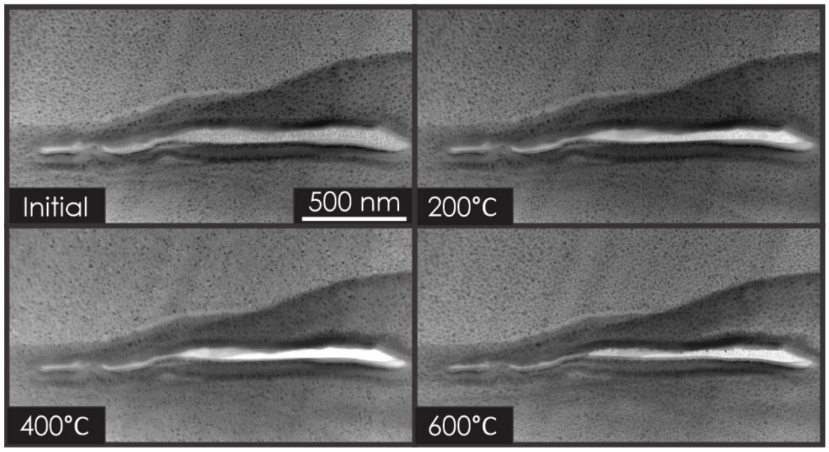

Figure 15. High resolution TEM micrographs of a thermal crack imaged at different temperature conditions. The closure of the cracks is more evident at the right side of the micrograph.

These results support the idea that thermal cracks are more susceptible to temperature changes and perhaps to neutron irradiation effects. Thermal cracks are believed to be closely related to thermomechanical changes induced by neutron irradiation. Figure 15 might provide evidence on why thermal cracks changes produced by neutron irradiation may play a significant role on the property and dimensional changes in nuclear graphite.

2.3.2.2 Microstructural Behavior with Annealing

Figure 16 shows nuclear graphite IG-110 thermally annealed at 2500°C for 24 hrs. then prepared to electron transparency via ion milling. Figure 16(a) shows a representation of the microstructure of nuclear graphites; crystallites are misaligned at various orientations and size, accompanied by porosity and nano cracks (Mrozowski). The indicated region of interest (arrow) is the edge of a crystallite oriented perpendicular to the c-axis. Figure 16(b) shows a high-resolution transmission electron microscopy (HRTEM) image of the indicated area in (a) where basal plane edges are observed to be rearranged into fullerene-like loops, the majority of which are multiwalled. Figure 16(c) shows additional evidence of the fullerene-like rearrangement throughout the interior of the specimen. Figure 16(d) shows an onion-like defect occurring within a quinoline insoluble particle.

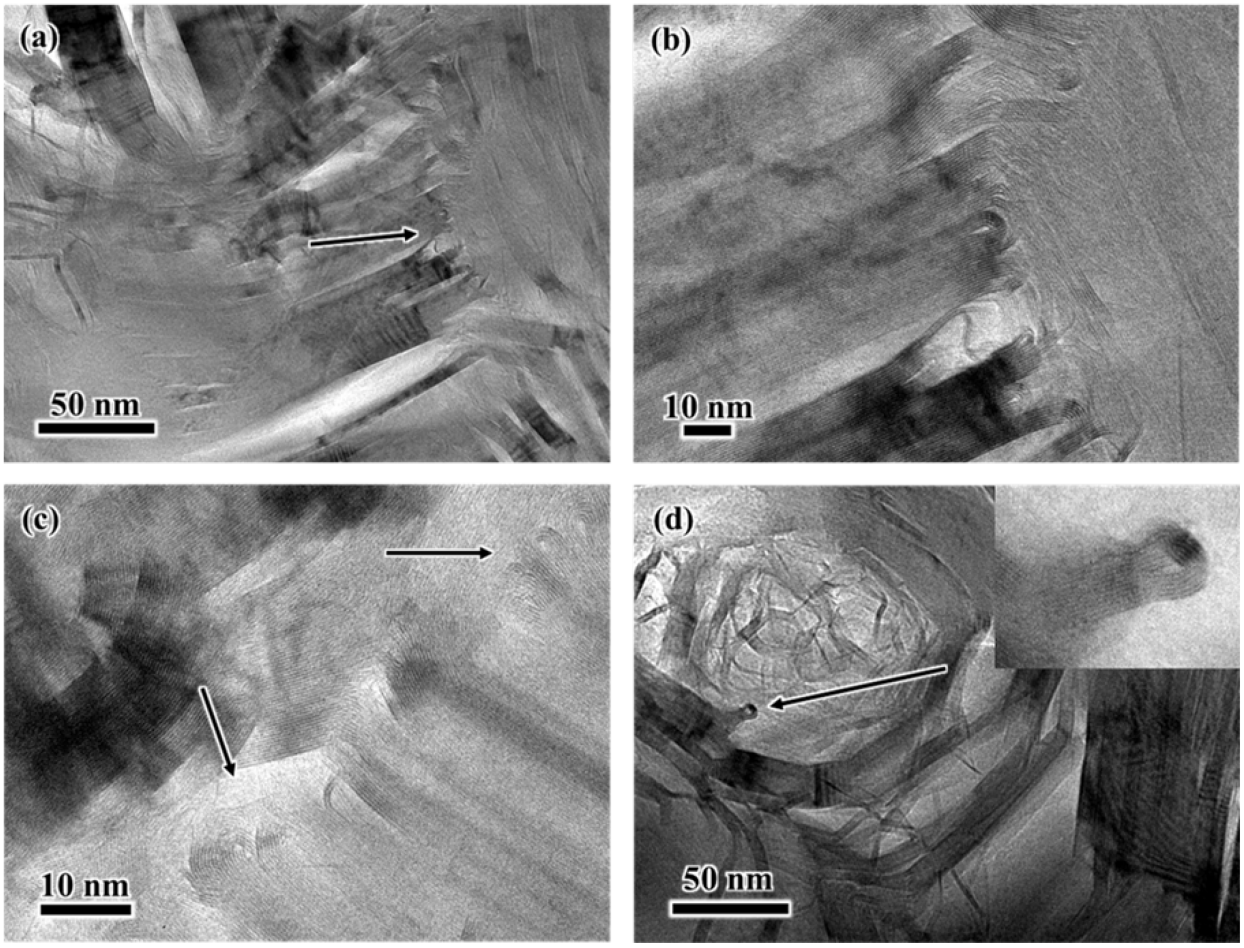

Figure 16. Bright field TEM micrograph of nuclear graphite IG-110 annealed at 2500°C for 24 h. Indicated in (a) is the edge of a crystallite oriented perpendicular to the c-axis. (b) shows a HRTEM micrograph of the indicated area of (a) which shows the rearrangement of basal plane edges into closed loops and fullerene-like structures. (c) and (d) show further evidence of fullerene-like structures occurring in the microstructure, in (c), concentrically rounded edges of crystallites and in (d), an onion-like defect occurring within a quinoline insoluble particle.

Figure 17 shows HRTEM micrographs of the post annealed TEM specimen. Figure 17(a) shows platelets of carbon directly on the specimen edge and morphology indicative of hexagonal rings; however, also shown as in Figure 17(b), are many porous fullerene-like structures. The structures are nearly identical to those reported by other studies of non-graphitizing carbons. Figure 17(c) shows closed curled edges of a crystallite oriented perpendicular to the c-axis similar to those shown in Figure 16, additionally, a multiwalled onion-like structure. One notable difference between the results shown is the observation of faceted edges. These faceted edges are believed to 'relax' due to ion-milling and result in the non-faceted rounded edges seen in Figure 16. Figure 17(d) shows the curling of basal plane edges and small fullerene like structures decorating the edge of the specimen.

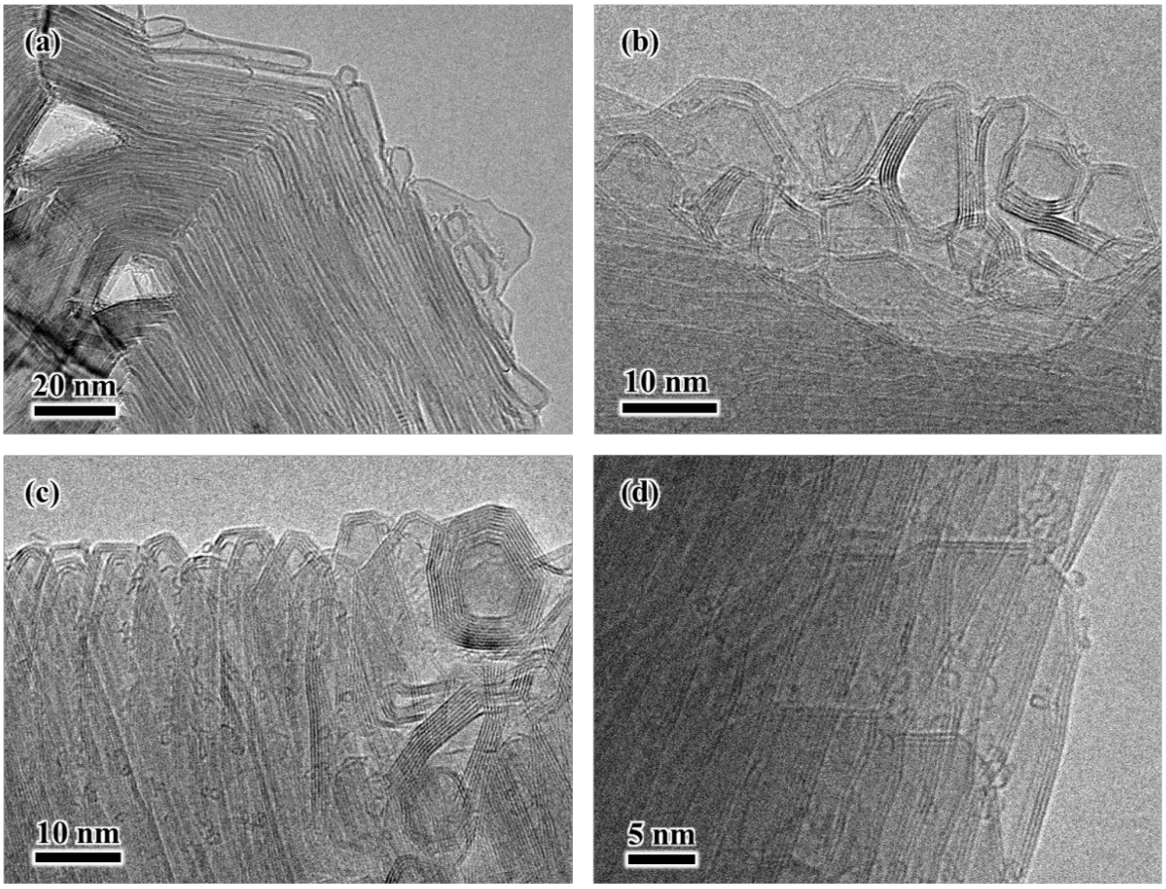

Figure 17. HRTEM micrographs of annealed IG-110. (a) shows the edge of the annealed specimen where fullerene-like structures are abundant. (b) shows further evidence of poorly graphitized phase. (c) shows the edge of a crystallite oriented perpendicular to the c-axis where all basal plane edges have rearranged into faceted closed structures. (d) shows a crystallite decorated with small fullerene structures.

2.3.2.3 Binary Random Field for Nuclear Graphite

2.3.3 Graphite Modeling

Recent graphite modeling efforts were focused in two main areas. The first area was the completion of the Level 3 milestone M3TG-21IN0501037. This report titled "Initial Developments in Modeling Graphite Behavior" on recent graphite modeling efforts conducted at INL was issued on time. The second area was the modeling of stresses in graphite which are generated in a reactor environment. Understanding and modeling these stresses in graphite is essential to ensuring that a graphite component can be safely utilized in a nuclear application.

Article HHA-3000 in Section III, Division 5 of the ASME BPVC provides design rules for graphite core components. One of the requirements set forth in the design by analysis approach is that either the simplified assessment or full assessment is passed. In order to use either of these assessments, the stress state in a component must be determined. This has prompted the development of modeling capabilities associated with determining the stress state in an oxidized graphite component.

Oxidation, which can occur in a reactor, is known to significantly affect graphite's behavior. It is addressed in HHA-3141 of Section III, Division 5 of the ASME BPVC that the mass loss profile, caused by oxidation, must be analyzed. Determining the mass loss profile in a component is of interest because the local mass loss will directly influence the local properties in a component. Ultimately this means that two components with the same geometry and total mass loss can behave differently if the mass loss profiles differ.

To simulate the stresses generated in an oxidized graphite component, the strains, temperature, and mass loss are state variables. The local material properties can be a function of one or more of these state variables. These parameters are essential to include in the model because as graphite oxidizes and changes temperature, the material properties can change drastically. This is evident in Figure 18, which shows some of the material property fits which were generated in order to run example problems.

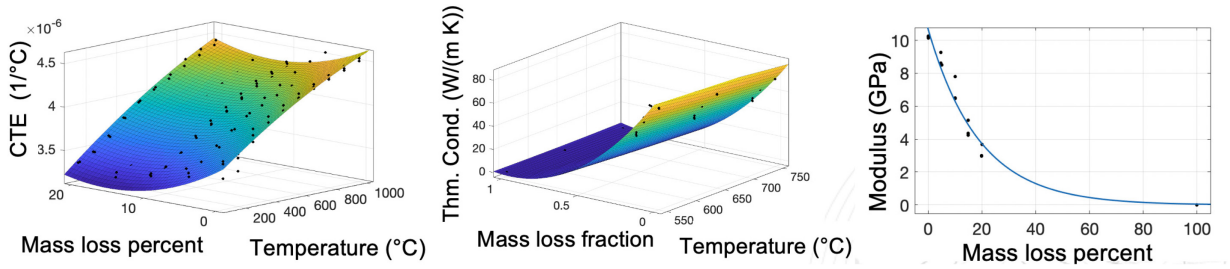

Figure 18. Coefficient of thermal expansion (left), thermal conductivity (center), and elastic modulus (right) implemented in simulations in order to determine stresses generated in an oxidized graphite component.

This model was implemented in Multiphysics Object Oriented Simulation Environment (MOOSE), the finite element framework developed at INL. Several preliminary simulations were run, one of which is included here as an example problem. This two-dimensional example problem uses one sixth of a prismatic core fuel block as the initial geometry. This geometry is shown in the left image in Figure 19. Temperature boundary conditions were set so the holes containing the fuel rods had a surface temperature of 1000 K while the temperature of the coolant gas holes had a surface temperature of 950 K. While the temperature profile varied slightly during the simulation, a representative temperature profile is shown on the right side of Figure 19.

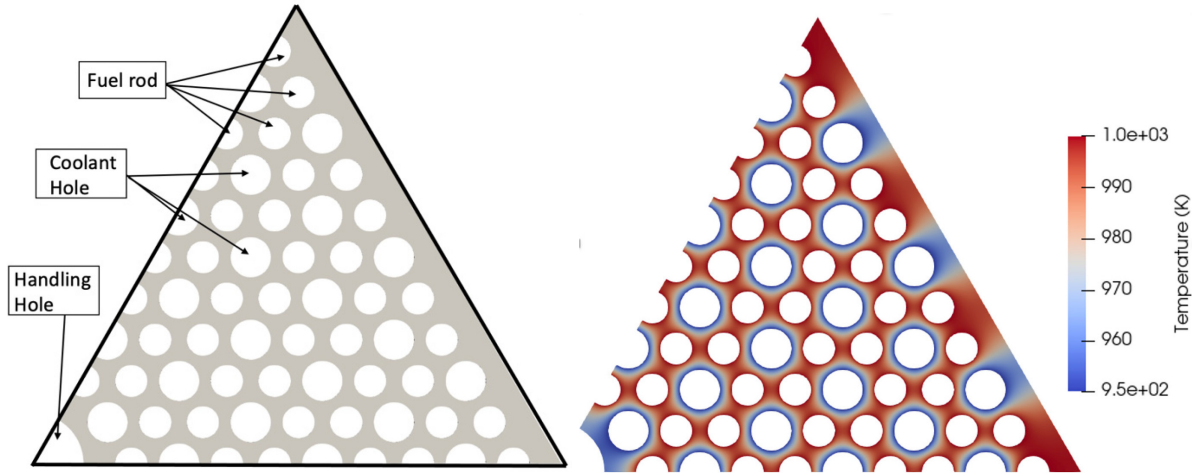

Figure 19. Example problem prismatic fuel block geometry (left) and temperature profile (right).

In an accident scenario, an oxidant may be present in the coolant gas. To incorporate this into this example problem, a constant O_2 concentration boundary condition was implemented on the coolant hole surface. This oxidant diffuses into the graphite and reacts to generate the density profiles in the graphite. The density profiles after 10 and 30 minutes are shown in the left column of Figure 20. The von Mises stress distributions generated by the variation in the temperature profiles at 10 and 30 minutes are shown in the right column of Figure 20.

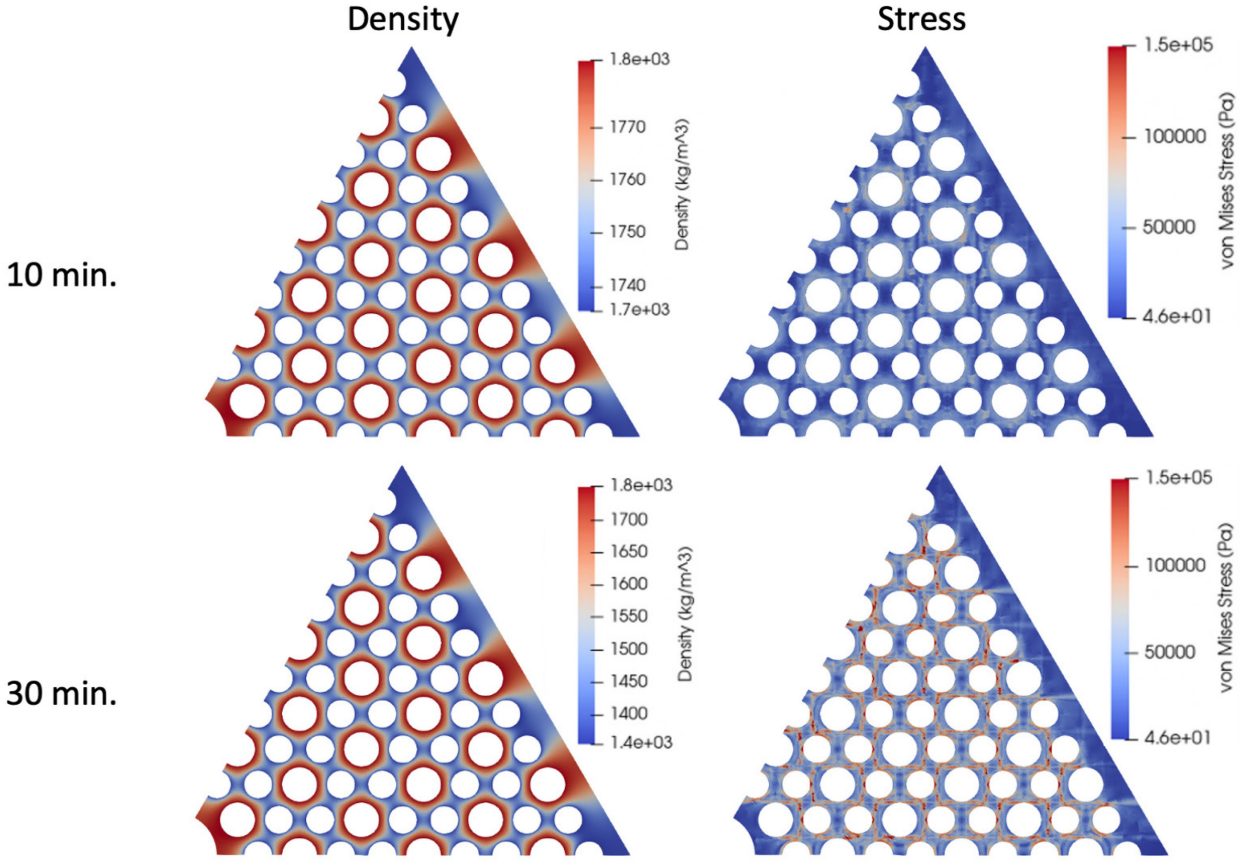

Figure 20. Density profiles from oxidation (left column) and stress distribution (right column) at 10 minutes (top row) and 30 minutes (bottom row).

The stresses computed at 30 minutes are shown to be slightly higher than those at 10 minutes, but this difference is not substantial. The primary behavioral difference is apparent when the strength of oxidized graphite is considered. Oxidation causes a significant drop in strength, so while the stresses don't significantly vary, the graphite oxidized for 30 minutes will have much less strength than the graphite oxidized for 10 minutes. In future work, stress distributions like those computed in this example problem will be implemented in the simplified and full assessments in the ASME BPVC.

2.3.4 Collaborations and Licensing: Graphite

2.3.4.1 ASME/NRC Activities

The second 2021 quarterly meeting of the ASME NDM WG was held virtually on May 11, 2021, again with large community participation with at least 20 attendees. The committee was well represented with a good spread between HTR vendors, material scientists and engineers, regulator individuals and international participants.

The task groups within the working group initiated, are getting up to speed on how to address the identified optimization areas through answering specific questions on the reviewed ASME BPVC Sec III.5 2017 ed which included the graphite code. The topical areas include:

- Irradiation dose limits and data interpolation vs extrapolation, led by Ms. J.W. Geringer,
- Defined Weibull and allowable stress calculations, led by Ms. A. Mack,
- Oxidation criteria in the code, led by Dr. C. Contescu,
- Deformation limits and the definition of "damage tolerance" led by Dr. M. Metcalfe,
- Irradiation data integration, led by Dr. W. Windes, and
- Molten Salt Reactor conditions and material properties affected as result, led by Dr. N. Gallego.

The objective of the task teams is to get experts with diversified background in the field (from national laboratories, universities and industry) together, to address key code criteria with supporting whitepapers by either expanding or revising the code where needed.

ASME codes and standards record 19-2805 on the elimination of fluence and historical dose units, affecting both graphite and composite core components, passed the BPV III vote and it was sent for ballot to the standards committee. Through record 21-557 limited data extrapolation was also determined to be permissible when generating irradiated material properties for a material data sheet for a graphite grade as required in HHA-2200(a) in accordance with the requirements of appendix HHA-II-4000. The draft Nonmandatory Appendices on Carbon-Carbon Composites, record 20-1307, received comments from its first WG-ballot which are being addressed. A community workshop on optimizing and modifying the Weibull analysis was held on April 28, 2021. Participants concluded that definite changes are required on the two parameter Weibull equations as defined in HHA-II-3100. However, although the code is conservative for any graphite grade, the code was found not to be equally conservative. A follow up task group meeting will be held. An oxidation task group meeting was held on May 20, 2021 to address the first question concerning graphite. Apart from obvious code changes like hydrogen does not cause oxidation and that radiolytic oxidation does not occur in high temperature gas cooled reactors, additional action is required on localized oxidation and the combined irradiation and oxidation effects. A whitepaper on "Damage Tolerance in the Graphite Cores of UK Power Reactors and Implications for New Build" was drafted and is being circulated for review.

Copyediting and formatting of document NTB-4-2021 titled “Background Information for Addressing Adequacy or Optimization of ASME BPVC Section III, Division 5 Rules for Nonmetallic Core Components” has been completed. The document has been sent to publishing and the revised expected release date is July 2021.

The next ASME BPVC week is scheduled for the last weeks in July and will be held virtually.

2.3.4.2 Oxidation Activities to support ASME Code: Bridging the gap between laboratory-scale oxidation tests and graphite oxidation specifications in the ASME BPVC Section III

Deterioration of nuclear graphite’s properties following oxidation by impurities in the helium coolant (chronic oxidation) or a postulated low probability event of air or steam ingress (acute oxidation) is a continuously expanding research field which resulted in several hundred publications in the open literature. Most of this research was performed at laboratory scale, using small graphite specimens and well-controlled conditions. The results show that oxidation behavior depends not only on graphite-specific properties but also on external factors characterizing testing conditions. Although a general understanding of the relative influence of these factors has emerged, transposing laboratory results into predictions for full-scale graphite components behavior is still not straightforward. Since oxidation experiments with full size graphite components are not feasible, modeling recommends itself as the best (and only) option. This direction has seen continuous progress in the U.S. and internationally. However, the results of predictive models are as good as the data used for input. The ASME code requires that all properties of graphite materials internal to the reactor core must be known in advance and listed in the Material Data Sheet. This includes mechanical and thermal properties of graphite materials with various levels of weight loss caused by oxidation. The Code then prescribes procedures for calculation of strength- and dimension reduction graphite components at representative conditions within the design-based parameter envelope. However, the current version of the Code is not clear on how to define oxidation levels and how to measure properties of oxidized graphite specimens. The Code does not currently recommend modeling for representation of oxidation effects. Such models should start by mapping local graphite properties as a function of oxidant penetration depth under the surface exposed to oxidant. Experience at DOE national laboratories (Brookhaven National Laboratory, ORNL, INL) and internationally demonstrates that such models are feasible, and they give concurring results.

To improve the representation of environmental effects (oxidation) on graphite components in HTRs, a Task Force on Oxidation was created by the ASME Non-Metallic Work Group. It is composed of subject matter experts from U.S. and U.K. with background on graphite oxidation kinetics and modeling, graphite structure, graphite manufacturing, and reactor damage tolerance. The mission of ASME Task Group on Graphite Oxidation is providing solid documentation on environmental interactions of HTGR nuclear graphite and recommending revisions and updates to regulatory specifications in ASME BPVC Section III articles related to graphite oxidation and its effects on graphite properties. The recommendations will be supported by peer-reviewed white paper(s) which will summarize the current understanding of oxidation behavior, its effect on mechanical and thermal properties, and ways to predict and prevent the negative consequences of postulated off-normal events. The white paper(s) will be made largely accessible to the international community by publication as an open distribution document.

During the period of references, the Task Group focused on assembling an information database from open domain publications (scientific and technical papers, review articles, technical memoranda, regulatory documents) related to environmental effects on graphite components in HTRs. This information will provide reference sources for an improved presentation of gas coolant – graphite interactions (oxidation) and of related property changes. It is expected that the literature review will indicate the need of revisions, clarifications, or updates to oxidation-related Articles in future editions of ASME BPVC Section III Subsection HH Subpart A. The new information will also be used to expand

Article HHA-B-3000, “Gas Coolant – Graphite Interactions (Oxidation)” and Article HHA-B-5000, “References”, in the Nonmandatory Appendix HHA-B, “Environmental Effects in Graphite”.

As a first step, the Task Group identified a few places where the current version of the Code (2019) is either incorrect or contains information not relevant to graphite-moderated HTRs (in particular, HTGRs and MSRs). They have been listed under the new record (21-1392) “Addressing oxidation issues in the code as it relates to graphite-moderated HTRs”. The proposed changes are as follows:

- Drop “radiolytic oxidation” from HHA-2230 and HHA-3140.
  - Motivation: Radiolytic oxidation is typical for CO_2-cooled AGRs in UK but it is not expected in HTGRs and MSRs that use high-purity He as coolant.
- Drop “hydrogen” from HHA-3141.
  - Motivation: Hydrogen cannot cause graphite oxidation (on the contrary, H_2 slows down oxidation by water).
- Add “moisture” in HHA-3141.
  - Motivation: Traces in the helium coolant will cause extremely slow, but continuous, chronic oxidation during normal operation during reactor’s service life.
- Add text to HHA-3141 to emphasize the localized character of oxidation, and therefore of the localized density profile that develops in the component’s subsurface penetrated by oxidant.

Motivation: Using modeling for mapping the profile of weight loss (or density) versus penetration depth of oxidant is essential for calculation of strength and geometry reduction in oxidized components (HHA-3141) as required for stress analysis (HHA-3215).

The propose changes will be discussed and balloted at the July 2021 meeting of Non-Metallic WG.

2.3.4.3 ASME Report on UK Damage Tolerance Experience in Graphite Cores

A draft white paper on damage tolerance in graphite cores of UK reactors and its implications for new builds has been developed and circulated for comment to ASME Nonmetallic WG members and interested participants. Highlights of this review include:

- All UK reactor designs share the same high-level nuclear safety requirements of being able to shut-down, cool and refuel the cores. These requirements relate to adequately maintaining the geometry of the core, which potentially may be affected by damage in the form of cracked graphite components.
- The graphite cores of Magnox gas-cooled reactors were not tolerant to cracked bricks because of associated impairments to coolant flow over the fuel and potential overheating of the fuel.
- The graphite cores of Advanced Gas-Cooled Reactors are broadly tolerant to the presence of large numbers of cracked bricks in terms of cooling because of the re-entrant flow design of the cores.
- Prediction of times to crack initiation and crack propagation in graphite components contain significant uncertainties and safety cases for continued operation of plant need to be additionally supported by inspection and monitoring data.
- Damage tolerance is design-dependent, and it is incumbent on designers to fully assess graphite core component functionality and the consequences of cracking.

2.3.4.4 ASTM

ASTM Symposium and Selected Technical Papers Publication

The ASTM event 'Symposium on Graphite Testing for Nuclear Applications: The Validity and Extension of Test Methods for Material Exposed to Operating Reactor Environments' under the auspices of the D02.F Subcommittee on Manufactured Carbon and Graphite Products' is scheduled to take place on September 23 and 24, 2021. This virtual event hosted by ASTM will include thirteen presentations covering measurement strategy and characterization, MSRs, oxidation and physical and mechanical property measurements that will be published in a peer reviewed ASTM volume of Selected Technical Papers in 2022.

2.3.4.5 International Atomic Energy Agency Knowledgebase and GIF Activities

Preparations for the 2021 the INGSM meeting are underway. The meeting will be held virtual in September 2021. The meeting website is up and running and the call for papers have been distributed.

2.3.5 Construction of MacroRaman Spectrometer

The construction of macroRaman spectrometer was completed, enabling us to characterize the microstructure of nuclear graphite on a larger scale to alleviate the impact of graphite spatial inhomogeneity.

Raman spectroscopy has been a powerful tool to examine the microstructure of graphite. Notable peaks, corresponding to the photons inelastically scattered by various phonons, appear in the Raman spectrum, from which a wealth of information on graphite, including crystallite size, stacking order, sp2/sp3 bond ratio, can be extracted. The ease of operation, little specimen preparation, and nondestructive features make Raman spectroscopy particular suitable for the studies on nuclear graphite. Nuclear graphite is in composite form, composed of multiple constituents with distinctive properties. Even for the same type of constituent, e.g., filler particle, there are also a wide distribution of morphologies that originate from the fabrication process. As a sequency, our initial results on graphite specimens, taken on a microRaman spectrometer with spot size about 1 μm, show significant scattering among measurements taken at different spots. For some key parameters, such as peak ratio, the obtained standard deviation sometimes exceeds the mean value, making it difficult to draw meaningful and generalized conclusions.

To alleviate the impact of spatial inhomogeneity on the Raman signal, we proposed to construct a macroRaman spectrometer that utilizes a much larger spot to excite Raman signal, achieving averaging over a larger volume of specimen. The diagram of our setup is presented in Figure 21a. The setup is built around three parabolic mirrors (PM) that facilitate the collection of Raman scattered photons. Several mirrors direct the excitation laser beam (532 nm) to the specimen surface. A focusing lens is placed in the light path to adjust the laser spot size on the specimen surface. The spot size is on the order of mm. As the specimen is the focus of PM1, the diffusively scattered phonons can be collected by PM1 and directed to PM2 in the form of collimated beam. After focusing and defocusing by PM2 and PM3, the diameter of the collimated beam is decreased to 1 inch, and the beam is fed to a spectrometer for analysis.

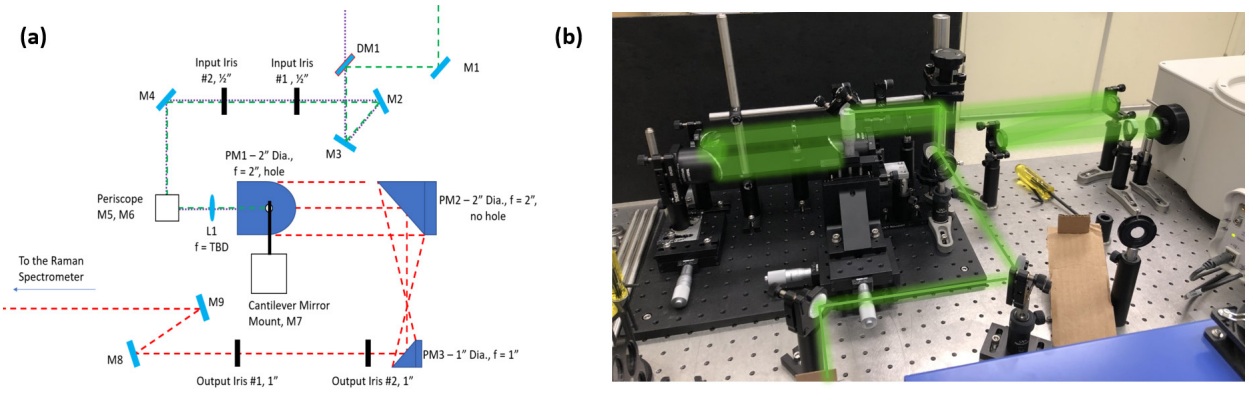

Figure 21. (a) Diagram of macroRaman spectrometer; (b) experimental setup of macroRaman spectrometer.

Tests on the macroRaman spectrometer were conducted on graphite and silicon. In Figure 22a, the Raman spectrum on silicon shows a prominent peak at 520 cm^{-1}, in agreement with the literature results. This demonstrates the reliability of our macroRaman spectrometer. In addition, three Raman spectra were collected on different spots of graphite NBG-18 under the same condition and are presented in Figure 22b. In contrast to our previous measurements with huge scattering, the result of macroRaman spectrometer displays consistent features across different measurements (Table 1). For example, the D and G peak ratio has a mean value of 0.74 with standard error of 0.1. The error is only 13.6% of mean value, confirming that the scattering is much reduced.

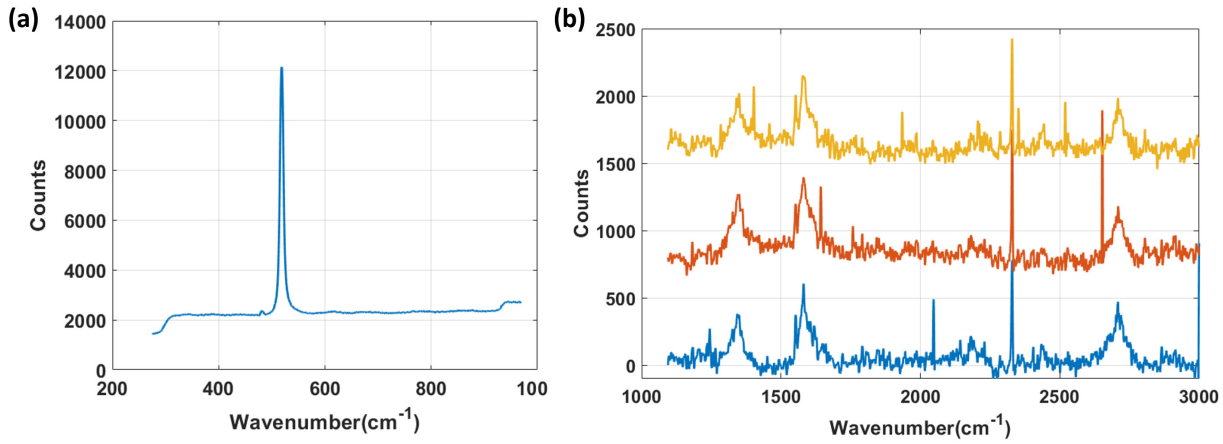

Figure 22. Raman spectrum collected on macroRaman spectrometer. (a) silicon, (b) graphite NBG-18.

Table 1. Summary of results from macroRaman spectrometer on graphite NBG-18.

Measurement	1	2	3
Amplitude (D peak)	329.4	393.4	288.4
Amplitude (G peak)	448.9	473.4	454.0
D and G peak ratio	0.73	0.83	0.64

2.3.6 Measurement of Thermal Diffusivity on Graphite Specimens Using Photothermal Radiometry

Thermal diffusivity of graphite determines how fast the energy generated in the nuclear fuels is conducted to the coolant, and thus is a key material property in nuclear reactor design. The thermal diffusivity of four major grades of nuclear graphite (2114, IG-110, NBG-18 and PCEA) were characterized by two methods, laser flash (LFA) and photothermal radiometry (PTR). Both methods employ infrared detector to measure the temperature changes under the excitation of laser beam (Figure 23) and require comparing the experimental signal with a heat transfer model to derive the specimen thermal diffusivity. LFA measures the time domain temperature rise at the rear surface of a specimen, while PTR measures the spatial domain temperature rise near the laser spot. For LFA measurement, a predefined specimen geometry is required, while for PTR, access to the rear side is not necessary.

Table 2. Thermal diffusivity of major grades of graphite measured by LFA and PTR.

	2114	IG-110	NBG-18	PCEA
D ($mm^2 \cdot s^{-1}$, LFA)	80.06±0.30	100.62±0.52	105.78±0.56	126.77±1.67
D ($mm^2 \cdot s^{-1}$, PTR)	79.11±4.65	89.06±6.51	91.97±11.20	103.46±21.07

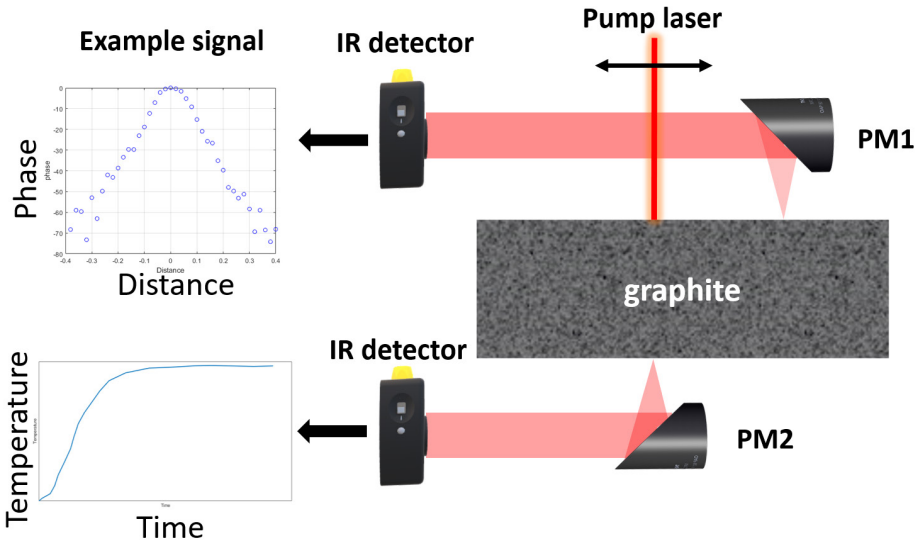

Figure 23. Diagrams of lash flash and photothermal radiometry methods.

The measurement results of both methods are summarized in Table 2. 2114 has the smallest thermal diffusivity, whereas PCEA has the largest diffusivity. The diffusivities of IG-110 and NBG-18 fall in the middle of the above range. In addition, except on 2114, the diffusivities obtained using both methods are generally not the same. The result of PTR is usually 80-90% of that from LFA. No conclusion on the reason for the discrepancy is drawn yet, but it is believed due to the microstructural features of graphite specimens. 2114, the finest grain graphite, shows no difference between the diffusivities from two methods. For the rest of graphite specimens with larger grains, the difference is persistent.

For More Information:

William E. Windes (william.windes@inl.gov)
Michael D. Davenport (michael.davenport@inl.gov)
Rebecca E. Smith (rebecca.smith@inl.gov)
Joseph L. Bass (joseph.bass@inl.gov)

Philip L. Winston (philip.winston@inl.gov)
Austin C. Matthews (austin.matthews@inl.gov)
Jason V. Brookman (jason.brookman@inl.gov)
Tommy V. Holschuh, II (tommy.holschuh@inl.gov)
Yuzhou Wang (Yuzhou.Wang@inl.gov)
Steve Johns (stevejohns@u.boisestate.edu)
Martin Metcalfe (martin.p.metcalfe@gmail.com)
Cristian Contescu (gallegonc@ornl.gov)
J. Wilna Geringer (geringerjw@ornl.gov)
Ryan Paul (paulrm@ornl.gov)
David Arregui-Mena (arreguimenjd@ornl.gov)
Nidia C. Gallego (gallegonc@ornl.gov)

2.4 Design Methods and Validation

2.4.1 RELAP5-3D Simulation of PG-27 Test at the HTTF Facility

During this quarter, the DOE milestone on the RELAP5-3D code qualification using HTTF data has been finalized. This milestone looked at test PG-27 conducted in the HTTF. The highlights of this study are summarized here.

The HTTF OSU is a quarter-scaled integral-effect test facility designed to examine the transient phenomena occurring in a Modular High-Temperature Gas-cooled Reactor. It is specifically designed to handle the Pressurized Conduction Cooldown (PCC) and Depressurized Conduction Cooldown (DCC) events. The PCC event is an accident scenario in which there is a loss of the forced convection of the coolant through the system. However, the pressure boundary remains intact. This study focused on the RELAP5-3D simulation of the PG-27 test (PCC phenomena) and the sensitivity of those simulations from the material properties and primary helium mass flow rate standpoint. The aim is to capture a reasonable 1D picture of a 3D phenomena. The code is able to capture the detailed 1D physics accurately. However, input parameters to the code (i.e., the primary mass flow rate, refractory material thermal conductivity, and heat capacity at elevated temperatures) impact the fuel temperature the most.

The base case (see Figure 24) shows a decent agreement with the overall progression of the transient as described by the comparative line plots tracked in the Core Block #3 and Primary Sector #5—which is the location for measuring the ceramic block temperature.

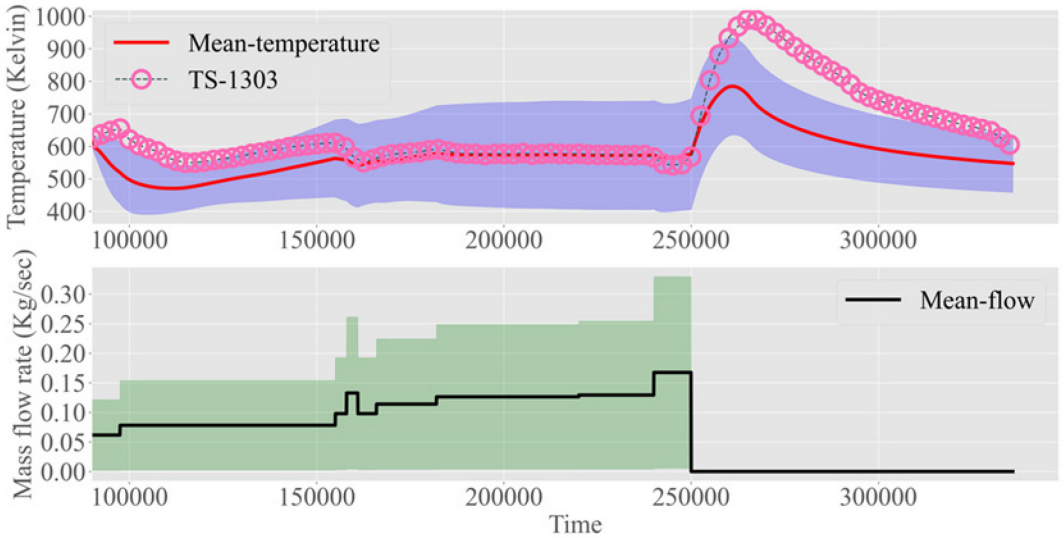

Figure 24. Statistical variation of temperature in Core Block #3 and Primary Sector #5 owing to the variation in the flow rate. The bands show $\mu \pm 2\times\sigma$.

The code was able to simulate the heating of the core and the rise in the solid temperature as soon as the circulator goes offline. However, certain discrepancies are obvious. The heating was not perfectly emulated and the temperature started to go up at around 140,000-time step. It is worth mentioning that no helium mass flow rates were measured during the test. The simulation results indicate that the modeled helium flow rate is relatively low. Therefore, the helium mass flow rate was increased in a sensitivity study. Higher helium mass flows correctly emulate the heating of the core. The correct storage of energy into the system during the heating up phase leads to the right progression of the transient later. Nevertheless, the increased helium mass flow rate leads to a suppression of the peak temperature observed during the transient progression while the point where the transient starts is correctly captured. To understand the effect of conductivity on the response variable, we decided to keep the flow fixed at the base mass flow rate and vary the conductivity. These results are shown in Figure 25. From the visual inspection, it is obvious that the response variable shows more diffusive behavior when the flow rate varies. Therefore, the exact flow rate computation is very important to understand the overall physics of this conduction dominant experiment.

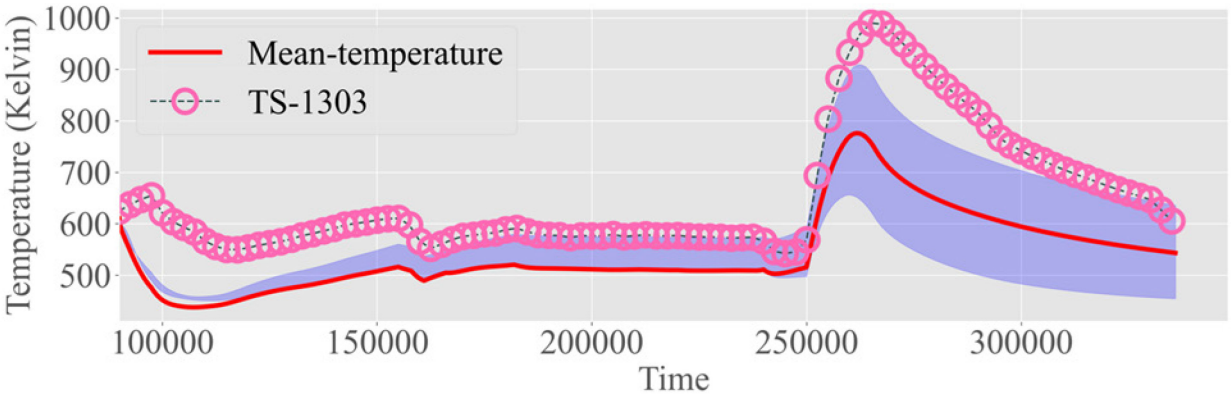

Figure 25. Statistical variation of the temperature in Core Block #3 and Primary Sector #5 owing to the variation in the conductivity. The bands show $\mu \pm 2\times\sigma$.

The computational model shows good overall agreement with the general data trend. Some discrepancies are obvious because of the parametric uncertainties in the model. They arise because of the two main factors; the calculation of the helium circulator mass flow rate and of the graphite conductivity. Getting the exact time-varying rate of the mass flow rate and the temperature-dependent profile of the material conductivity is an essential step to exactly match the conduction-dominant physics of the experiment.

2.4.2 Severe Accident Heat-Removal Testing

Effort on the NSTF program during the third quarter of FY21 saw completion of three data quality matrix tests in which the test facility was operated at varying two-phase boiling conditions to examine the influence of single-variable parameters on behavior and stability. Additionally, though testing is scheduled to continue until the September timeframe, planning efforts began in parallel for a facility maintenance period scheduled to begin early FY22. This shutdown, anticipated to extend four months, will be used to repair the faulted Guard heaters, examined the cavity interior, and collect emissivity measurements of the test section and heated surfaces.

The final test case within the restricted steam outlet parameter series was successfully performed early in the quarter. This series was established to examine the influence of varying levels of elevated systems pressures on two-phase operation. The most recent case, DataQuality068, was conducted with the highest system pressures observed to date, peaking at nearly two atmospheres within the gas space of the primary tank, Figure 26. In addition to completing the final test within the steam outflow parametric series, this case was extremely valuable in providing data for understanding of the instability mechanisms and re-stabilization conditions for the test loop.

Within the system inventory and tank volume parametric, an additional matrix test, DataQuality069, was conducted and successfully completed by the experimental team. This was an extended duration boil-off test with the loop beginning at 55% initial fill, and operated in a transient, two-phase mode of operation. Due to large voiding in the chimney region, swelling of this hot leg allowed the loop to flow continuously even as the level within the tank fell below the chimney inlet. After nearly eight hours of operation, flow continued to be observed even as the level fell 35-inches below the chimney inlet, with only approximately 20% of the tank inventory remaining, Figure 27.

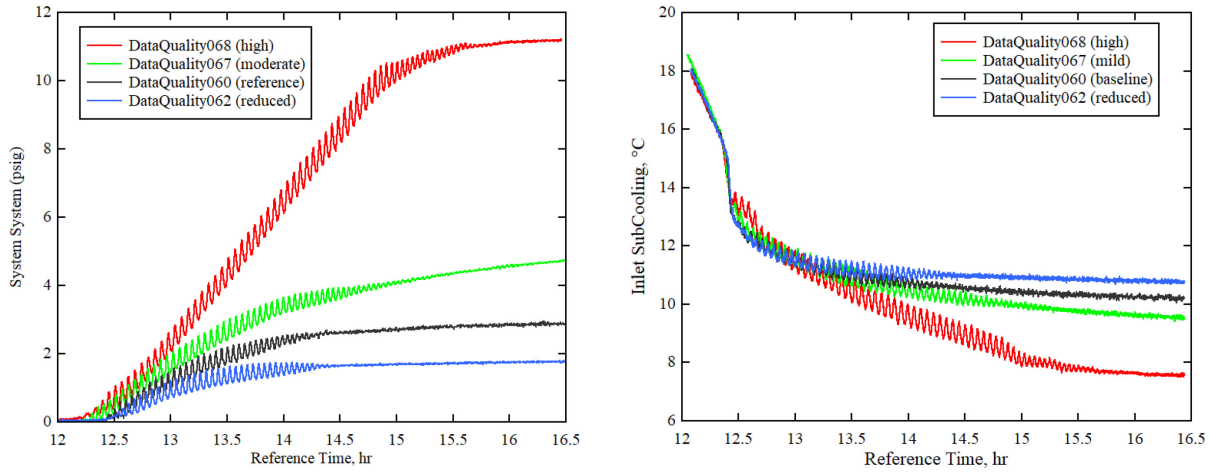

Figure 26. Gas space pressure and fluid outlet temperatures at varying levels of elevated system pressure.

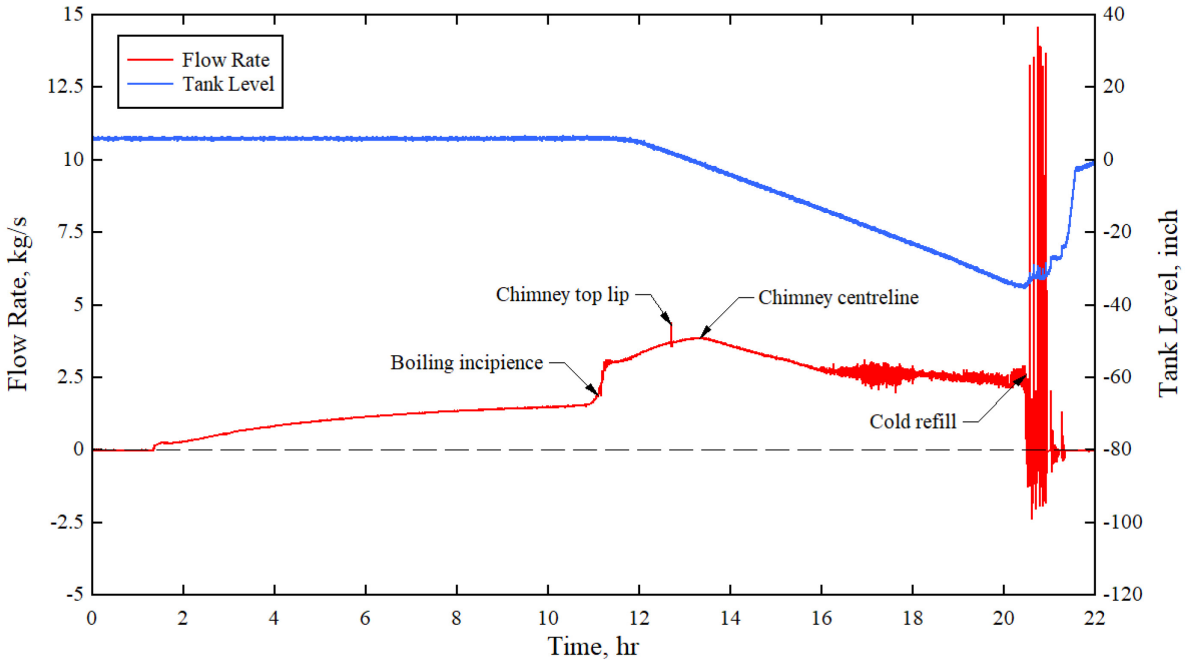

Figure 27. Time history of system flow rate and inventory level during an extended boil-off test. Tank level referenced to centerline of chimney inlet.

A third data-quality matrix test, DataQuality070, was conducted and successfully completed by the NSTF experimental team. This case was performed at baseline test conditions, modified to examine the influence of power at the lowest levels specified by the full scale concept. These are defined by "normal conditions", where the Reactor Cavity Cooling System receives a heat load of 1.4 MW_t in the full scale, or 34.4 kW_t in the NSTF. The facility ran in a transient mode of operation for a period of 25 hours and 13 minutes, during which the test acceptance criteria were successfully met, Figure 28. Currently the data is being reviewed, and it is expected that the team will release a preliminary test acceptance report for successfully completing this matrix test. Close-out of the power parametric test series will also require completing the last very high-power test, which will be held off until after the maintenance window and repair of the two faulted heater zones.

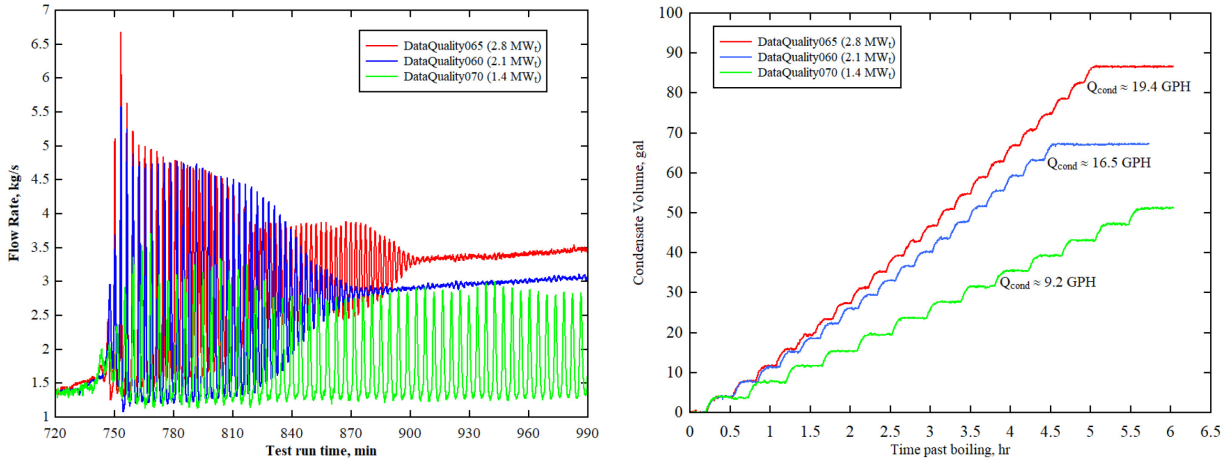

Figure 28. Comparison of system flow and boil-off condensate rate at varying power levels.

Preparations continued for the planned maintenance period, scheduled to begin in early September 2021 and extend until the December timeframe. This period will be used to repair the faulted Guard heaters, examined the cavity interior, and collect emissivity measurements of the test section and heated surfaces. A significant portion of our outer insulation panels will need to be removed to expose the guard heater zones, so the team is preparing for an erected scaffold spanning the height of the heated cavity.

For More Information:
Darius Lisowski (dlisowski@anl.gov)
Aaron Epiney (aaron.epiney@inl.gov)

3. 90 DAY LOOK AHEAD

3.1 Important Activities

3.2 Fuels Development

- Complete external visual exams and PGS of AGR-5/6/7 Capsules 3, 4, and 5 at INL.
- Complete final Phase III qualifications of the AGR-5/6/7 disassembly equipment at INL.
- Begin disassembly of the first segment of the AGR-5/6/7 test train at INL.
- Complete a reirradiation and heating test of an AGR-3/4 compact using the Neutron Radiography Reactor and Fuel Accident Condition Simulator furnace at INL.
- Complete analysis and reporting of ORNL FITT oxidation tests of AGR-2 UCO Compact 5-4-2 particles.
- Complete ORNL burnup analysis of AGR-3/4 Compacts 1-4 and 7-4.
- Complete upgrades of ORNL Core Conduction Cooldown Test Facility in preparation for AGR-5/6/7 safety testing.
- Disposition of all residual highly-enriched, low-enriched, natural, and depleted uranium materials stored at BWXT-Nuclear Operations Group will be completed.

3.3 High-temperature Materials

- Prepare background document on the 304/316 life extension proposal.
- Submit proposal for 304/316H life extension to 500,000 hours to ASME committees.
- Run additional crack propagation practice tests to compare with previous studies.
- Investigate gas chromatograph and verify functionality of environment testing capabilities.
- Sustain ongoing creep-rupture tests of Alloy 617 specimens containing various geometric discontinuities. The data will be analyzed as tests finish. Metallography and optical microscopy will be used to characterize specimens of interest.
- Reload and restart the interrupted creep-rupture test (800°C, 60 MPa) of a base-metal V-notch specimen. The expected life is 8,000 hours. The test was interrupted after 2,000 hours of testing.
- Analyze XCT data from the creep-fatigue test (850°C, $\varepsilon = 0.3\%$, 30 min hold) of a cross-weld specimen with Alloy 617 base and filler metal. The weld was centered with respect to the extensometer and reduced section. The termination criteria for this test was met after three cycles.

- Analyze the single-bar Simplified Model Test test data from the Alloy 617 specimen tested at 950°C with a virtual strain of 0.7% and a 10-minute hold. The test ran for 704 cycles.
- Initialize program to weld Alloy 800H with a matching filler metal using gas tungsten arc welding. Welding will need to be in accordance with Section III, Division 5 and Section IX. As a result, the weld operator(s), procedure, and performance need to be qualified. An INL weld specification will be developed.
- Continue efforts to set up a subcontract to hire a consultant to leverage European syngas industry experience of using matching consumables for welding Alloy 800H.
- Finalize the report titled "Report on Current Assessment of Overmatch Weld (Alloy 617) for Alloy 800H Life Extension." This report is a milestone deliverable.
- Draft and finalize a report titled "Recommendation for Limiting Conditions for ASME BPVC Section III Division 5 Allowable Stress Criteria." This report is a milestone deliverable.
- Participate at the July 2021 ASME Pressure Vessels & Piping Conference.
- Participate at the ART Gas-Cooled Reactor Program Review.
- Participate at the July ASME BPVC Week which will be held virtually.

3.4 Graphite Development and Qualification

- Conduct novel mechanical serial-sectioning combined with optical microscopy on nuclear graphite samples and compare with XCT scan results to investigate the microstructure of graphite.
- Resolve dose rate determination and complete documentation to allow shipment.
- Provide data from the Nuclear Data Management and Analysis System showing relevant experiment FY21 cycle information and complete HDG-1 Irradiation and Support for 1 ATR Cycle in FY21, due June 30, 2021.
- Conduct low-loss electron energy loss spectroscopy of annealed then cut vs, cut then annealed nuclear graphite.
- Complete characterization via TEM of nuclear graphite creep specimens.
- Complete draft manuscript of the microscopic response of thermally annealed nuclear graphite.
- Receive preliminary gamma spectroscopy results from creep samples, shutter piston and fluence capsule from AGC-4.
- Couple graphite stress modeling results to ASME graphite component assessment methodology.
- Issue memo, "Status of Irradiated Graphite Oxidation Memorandum," by July 31, 2021.
- Issue memo, "Initial Split Disk Testing Results," by August 31, 2021.
- Issue report, "AGC Dosimetry Improvements" by August 31, 2021.
- The ASTM International Symposium on Graphite Testing for Nuclear Applications is scheduled for September 23 & 24, 2021 as a virtual event.
- The INGSM is scheduled for September 27-30, 2021 as a virtual event.
- Optimizing macroRaman spectrometer for better signal-to-noise ratio.
- Beginning integration of UV laser with the macroRaman spectrometer.

- Completing the draft for a journal article about microstructures and thermal diffusivities of four grades of nuclear graphite.

3.5 Methods

- Follow-up on the HTTF benchmark meeting action items.
- Submit DOE FY21 milestone report on HTTF PG-27 using RELAP5-3D.
- Conduct final matrix test for FY21, then begin preparations for shutdown and maintenance period.